Towards Dexterous In-Hand Manipulation through Tactile Sensing

Zur Erlangung des akademischen Grades Doktor-Ingenieur (Dr.-Ing.)
genehmigte Dissertation von Filipe Fernandes Veiga aus Lissabon, Portugal
Tag der Einreichung: 31.07.2018, Tag der Prüfung: 22.10.2018
Darmstadt — D 17

1. Gutachten: Prof. Dr. Jan Peters
2. Gutachten: Prof. Veronica Santos

TECHNISCHE
UNIVERSITÄT
DARMSTADT

Inteligent Autonomous Systems (IAS)
Fachbereich Informatik

Towards Dexterous In-Hand Manipulation through Tactile Sensing

Genehmigte Dissertation von Filipe Fernandes Veiga aus Lissabon, Portugal

1. Gutachten: Prof. Dr. Jan Peters
2. Gutachten: Prof. Veronica Santos

Tag der Einreichung: 31.07.2018
Tag der Prüfung: 22.10.2018

Darmstadt — D 17

Bitte zitieren Sie dieses Dokument als:
URN: urn:nbn:de:tuda-tuprints-91802
URL: http://tuprints.ulb.tu-darmstadt.de/9180

Dieses Dokument wird bereitgestellt von tuprints,
E-Publishing-Service der TU Darmstadt
http://tuprints.ulb.tu-darmstadt.de
tuprints@ulb.tu-darmstadt.de

Die Veröffentlichung steht unter folgender Creative Commons Lizenz:
Namensnennung – Keine kommerzielle Nutzung – Weitergabe unter gleichen Bedingungen 4.0 International
https://creativecommons.org/licenses/by-nc-sa/4.0/

Erklärung zur Dissertation

Hiermit versichere ich, die vorliegende Dissertation ohne Hilfe Dritter nur mit den angegebenen Quellen und Hilfsmitteln angefertigt zu haben. Alle Stellen, die aus Quellen entnommen wurden, sind als solche kenntlich gemacht. Diese Arbeit hat in gleicher oder ähnlicher Form noch keiner Prüfungsbehörde vorgelegen.

Darmstadt, den 31.07.2018

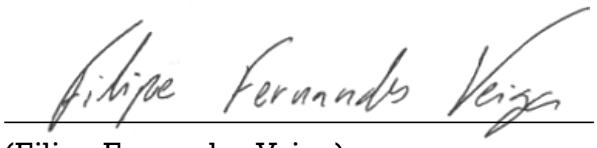

(Filipe Fernandes Veiga)

Abstract

Currently, robots display manipulation capabilities that translate into actions such as picking and placing objects or poring liquid from containers. For actions that require finer in-hand manipulation to reposition objects or to use them as tools, robots are still not proficient enough. These shortcomings become even more apparent when considering the ease with which humans perform such manipulations on a daily basis, and while these limitations are not addressed, robots can not truly aid humans with their daily activities.

The scope of possible interactions and the high dimensionality intrinsic to more dexterous robotic hands makes the manipulation problem hard to approach. Traditional control approaches to dexterous in-hand manipulation often work under the assumption that physical interactions, object properties, kinematics and dynamics of the robot can all be accurately modeled. Unfortunately, these modeling assumptions do not hold in most real environments, as uncertainty accumulates along the individual models. On the other hand, developing learning approaches that would generalize for all necessary manipulations proves difficult, as state spaces composed of the robots degrees of freedom and the necessary feedback channels often becomes too high dimensional and hence hard to explore.

For dexterous in-hand manipulation, one of the most notable differences when considering human and robotic systems is the role of tactile information. The human system is composed of thousands of tactile afferents that provide detailed information of what is occurring at each interaction point during the manipulation action. On the other hand, traditional robotic manipulation approaches often rely on vision or on force feedback, either lacking information collected directly at the contact interaction or the various forms of information provided provided by tactile feedback.

In this thesis, we explore tactile sensing as a means to bridge the gap in manipulation skills between humans and robots. We do so by assessing how to extract relevant feedback signals from the high dimensional tactile spaces, by exploring how to distribute the manipulation problem complexity onto modular components and to use these components to enable the use of powerful machine learning approaches, without loss of generalization capabilities.

Chapter 2 will cover the recovery of relevant feedback signals from the tactile sensory information. Here, the desired signal is the state of the interaction between the robot and the object, particularly the knowledge of events such as slippage between the object and the finger surface. Through the use of machine learning, we predict such slip events in a manner that is generalizable to unknown objects. The ability to predict tactile slip allows analytically designed control solutions to stabilize objects when using a single finger. This is showed for cases where the opposing contact on the object is provided either by a static plane or by a human finger.

In Chapter 3, we explore and extend a neurophysiological research hypothesis to the robotics domain. This hypothesis states that for stabilizing objects in-hand, digits can

be controlled independently from each other, with no form of explicit coordination. Taking full advantage of the predictive slip feedback signals and ensuring smooth control responses by each of the finger controllers, we show that a stable grips on unknown objects emerge while controlling each digit independently. We show that coordination is achieved through the perturbations observed via the tactile feedback of each individual finger.

Finally, in Chapter 4, use the modular nature of the grip stabilization control to enable the learning of manipulation policies in a hierarchical control setting. Reinforcement learning is used to learn a high-level control layer that exploits a lower-level composed of modular controllers that ensure the objects remains within the grip while being manipulated. In addition, we show that such a hierarchy facilitates the transfer of high-level policies learned in simulation onto real systems by using the low-level as an abstraction of the tactile information.

Zusammenfassung

Derzeit zeigen Roboter Manipulationsfähigkeiten, die Aktionen wie das Aufnehmen und Platzieren von Objekten oder das Ausschütten von Flüssigkeit aus Behältern ermöglichen. Für Aktionen, die eine feinere in-Hand Manipulation der Objekte erfordern, um diese neu zu positionieren oder als Werkzeuge zu verwenden, sind Roboter noch nicht geschickt genug. Diese Mängel werden noch deutlicher, wenn man bedenkt, mit welcher Leichtigkeit Menschen solche Manipulationen täglich durchführen, und während diese Einschränkungen nicht adressiert werden, können Roboter dem Menschen bei ihren täglichen Aktivitäten nicht in vollem AusmaSS helfen.

Der Umfang der möglichen Interaktionen und die hohe Dimensionalität, die geschickteren Roboterhänden innewohnt, macht es schwierig, sich dem Manipulationsproblem zu nähern. Traditionelle Steuerungsansätze zur geschickteren in-Hand Manipulation funktionieren oft unter der Annahme, dass physikalische Wechselwirkungen, Objekteigenschaften, Kinematik und Dynamik des Roboters genau modelliert werden können. Leider halten diese Modellierungsannahmen den meisten realen Umgebungen nicht stand, da sich die Unsicherheiten entlang der einzelnen Modelle aufsummieren. Andererseits erweist sich die Entwicklung von Lernansätzen, die für alle notwendigen Manipulationen verallgemeinern würden, als schwierig, da Zustandsräume, die sich aus den Freiheitsgraden der Roboter und dem notwendigen Feedback zusammensetzen, oft zu hochdimensional und damit schwer zu erforschen sind.

Die Rolle der taktilen Informationen, ist für die geschickte in-Hand Manipulation einer der auffalendsten Unterschiede bei der Betrachtung von menschlichen und robotischen Systemen. Das menschliche System besteht aus Tausenden von taktilen Afferenzen, die detaillierte Informationen darüber liefern, was an jedem Interaktionspunkt während der Manipulationsaktion passiert. Andererseits verlassen sich traditionelle robotergestützte Manipulationsansätze oft auf Visuelles oder Kräfte Feedback. Oft fehlen hierbei die Informationen die direkt an der Kontaktstelle gesammelt werden, oder die verschiedenen Formen von Informationen die durch taktiles Feedback bereitgestellt werden.

In dieser Arbeit untersuchen wir die taktile Sensorik als Mittel, um die Lücke in der Manipulationsfähigkeit zwischen Mensch und Roboter zu schlieSSen, indem wir analysieren, wie man relevantes Feedback aus den hochdimensionalen taktilen Räumen extrahieren kann und indem wir erforschen wie man die Komplexität des Manipulationsproblems auf modulare Komponenten verteilt und diese Komponenten verwendet, um den Einsatz leistungsfähiger maschineller Lernansätze zu ermöglichen, ohne Verallgemeinerungsfähigkeiten zu verlieren.

Kapitel 2 behandelt die Rückgewinnung relevanten Feedbacks aus den taktilen sensorischen Informationen. Das gewünschte Signal ist hier der Zustand der Interaktion zwischen Roboter und Objekt, insbesondere die Kenntnis von Ereignissen wie z.B. den Schlupf zwischen Objekt und Fingeroberfläche. Durch den Einsatz von maschinellem

Lernen prognostizieren wir solche Gleitereignisse in einer Weise, die für unbekannte Objekte verallgemeinerbar ist. Die Fähigkeit, taktilen Schlupf vorherzusagen, ermöglicht analytisch entwickelte Kontrolllösungen zur Stabilisierung von Objekten bei Verwendung eines einzigen Fingers. Dies wird für Fälle gezeigt, in denen der gegenläufige Kontakt auf dem Objekt entweder durch eine statische Ebene oder durch einen menschlichen Finger erfolgt.
In Kapitel 3 untersuchen und erweitern wir eine neurophysiologische Forschungshypothese auf den Bereich der Robotik. Diese Hypothese besagt, dass zur Stabilisierung von Objekten in der Hand, Finger unabhängig voneinander gesteuert werden können, ohne explizite Koordination. Wir nutzen die Vorteile des prädiktiven Schlupf Feddbacks voll aus und sorgen für eine stufenlose Steuerung durch jede der Fingersteuerungen. Wir zeigen, dass stabile Griffe auf unbekannten Objekten entstehen, während jeder Finger unabhängig voneinander gesteuert wird. Wir zeigen, dass die Koordination durch die beobachteten Störungen über das taktile Feedback jedes einzelnen Fingers erreicht wird.
SchlieSSlich, in Kapitel 4, verwenden Sie die modulare Natur der Griffstabilisierungs Kontrolle, um das Erlernen von Manipulationsstrategien in einer hierarchischen Kontrollumgebung zu ermöglichen. Reinforcement Learning wird verwendet, um eine übergeordnete Steuerungsebene zu erlernen, die eine untere Ebene aus modularen Steuerungen nutzt. Die untere Ebene stellt sicher, dass die Objekte während der Manipulation im Griff bleiben. Darüber hinaus zeigen wir, dass eine solche Hierarchie die Übertragung von übergeordneten Strategien, die in der Simulation gelernt wurden, auf reale Systeme erleichtert, indem sie die untere Ebene als Abstraktion der taktilen Informationen verwendet.

Acknowledgements

Over the course of by PhD, several people supported me in many ways. Without these friends, family and colleagues this thesis would have not been possible. Thus, I would like to thank:

- Jan Peters for is patience, guidance and advice. His supervision has made me a better researcher but also a better professional and, without him, it would have been hard to believe in myself when I needed to.
- Benoni B. Edin for great discussions and for his though reviewing nature, always considering every detail, teaching me how to express myself very clearly and precisely.
- Prof. Jan Peters and Prof. Veronica Santos for being my thesis referees.
- Prof. Stefan Roth for heading my thesis committee and Prof. Oskar von Stryk, Prof. Reiner Hähnle and Prof. Andre Seyfarth for agreeing to be members of the committee.
- My co-authors, from a variety of great collaborations, particularly Jan Peters, Gerhard Neumann, Tucker Hermans, Benoni B. Edin, Riad Akrour, Herke van Hoof, Roberto Calandra, Rudolf Lioutikov and Zhengkun Yi.
- My office mates, Roberto, Takayuki, Serena and Samuele with whom I learned a bit of Italian and Japanese while enjoying a great working environment.
- Gerhard, Elmar, Oliver, Christian and Herke, for the guidance as I was begging my PhD and the advice throughout, each making me feel part of the group in his own way.
- Boris, Patrick and Rudolf for keeping me alive during climbing and for great the discussions that followed each climbing session.
- My colleagues Joni, Hany, Boris, Samuele, Simone, Marco, Gregor, Oleg, Daniel, Dorothea, Svenja, Fabio and Michael for their companionship.
- Alexandros for the great and not so great dinners, for the car rides, the work discussions and for always being there when I needed my happy Greek friend.
- Roberto and Radica becoming part of my family and letting me become a part of theirs. They were always there for me and I hope they always will be.
- Rudolf, the brother I met only five years ago. During these years, we laughed, worked, traveled and drank together, and his presence, support and mean comments were a constant that I could always count on, and that I hope remain for many years following.
- Lisa, my new little sister for her support, for always spoiling me with sweets and for being the greatest flatmate I have ever had.
- Cristina, Filipe, Valter, João Paulo for always making me feel as if they are there, no matter the distance between us.
- My Mom and Grandmom, for their love and support and for being examples of selfless care for others. Together with my Dad and Granddad, they have made me what I am today and keep pushing me to be the best I can be.
- Catarina for her love and for making my life crazier and happier, while supporting me, being insanely picky with words, creating the most ridiculous hashtags and making me laugh every day.

Contents

1 Introduction

A learning agent becomes able to reason about its surroundings by interpreting what he perceives and by being able to act and explore the consequences of its actions. Having such agents amidst humans, aiding them with day to day tasks, can reshape society and greatly improve human quality of life. While they could be capable of fulfilling such a role, the current unrealized potential of robots prevents them from having a greater impact in society. Currently, robots still struggle with perceiving and interacting with their surroundings outside of controlled environments, a fact that is specially prominent when comparing human and robot behavior. The skill gap between humans and robots is particularly evident for dexterous in-hand manipulation actions, where objects are manipulated within the fingers of a multi-fingered hand. This form of manipulation allows humans not only to interact with a multitude of objects, but also to use them as the tools necessary to solve a wide range of tasks. Hence, as long as robots lack robust dexterous manipulation skills, they will be unable to solve or aid humans in solving their day to day tasks, and the full potential of robotics will remain unexplored.

In humans, manipulation skills are heavily tied to the sense of touch [40]. Tactile information plays a major role not only in perceiving object properties such as texture, thermal conductivity and surface temperature, contact surface compliance, size and shape [49], but is it also crucial for controlling the manner in which objects are manipulated [41]. During precision manipulation actions, different types of mechanoreceptors in the human fingertip [42] provide rich tactile information, allowing humans to perceive both continuous and instantaneous changes in their interactions with the environment. For example, consider a pick and place task where an object is grasped, lifted of its supporting surface, transported within a stable grasp and placed on a different supporting surface. By observing the deformation profiles during the first milliseconds of making contact with the object, humans are able to estimate the friction at the contact surface [41] allowing them to adjust the forces applied by each of the fingers prior to lifting the object [43]. As the object is lifted, changes in the tactile signals are used to detect the instant where the contact is lost with the external support surface [89], allowing for a smooth transition between the lift and transport phases. During the transport phase, abrupt changes in the grip state can be detected by observing sharp transitions in the tactile signals and can trigger corrective actions if these changes are undesirable (for example if slip is occurring at one of the contact surfaces) [41]. Finally, as the object is placed on the new supporting surface, the ability to detect the instant that contact is made between the two gives humans the ability to place objects delicately, without damage to the object or the supporting surface. To cope with all these continuous and event based changes to the contact state, and considering that instantaneous events such as slip are highly detrimental to manipulation actions, merely reacting after the occurrence of some of these events could prove insufficient. Considering the complex manipulation actions that humans

are capable of performing suggests that they are able to manage continuous contact properties such as applied force while anticipating and reacting to undesirable events before they actually occur [41].
The role of tactile information in human manipulation has not gone unnoticed, and in recent years several sensing technologies capable of providing robots with similarly rich tactile information have been developed [30, 19]. Nonetheless, integrating such information in its raw form would increase the complexity of a control problem where multiple degrees of freedom are controlled while taking into consideration finger object interactions, finger coordination, grip configuration and object properties. Hence, selecting which type of information is useful for each manipulation task is still and open problem, reflected by the wide range of sensing technologies proposed [96, 45] and empathized by the increasing dimensionality of the tactile signals provided by more recent sensing technologies [50, 97, 95].
In this thesis we explore tactile information as the means to endow robots with the necessary dexterous in-hand manipulation skills that generalize across several tasks. To cope with the tasks complexity, we propose several methods where relevant feedback signals are extracted from the tactile information and the control problem is partitioned by exploring findings from human neurophysiological research that suggest that human manipulation control is distributed over multiple control layers [25, 10, 28]. Together, these methods enable the use of reinforcement learning techniques to learn complex in-hand manipulation movements in simulated environments while ensuring that resulting controllers can also be deployed in real robot platforms.

1.1 Contributions

Our efforts to reduce the skill disparity in dexterous in-hand manipulation between robots and humans are described in the following chapters of the thesis. In Chapter 2 we present an approach to predict object slippage from tactile information. With the developed slip predictors we explore a modular grip stabilization control approach that is presented in Chapter 3. Finally, Chapter 4 introduces a hierarchical control decomposition for the dexterous in-hand manipulation problem that takes advantage of the modular stabilization controllers. The key contributions of each of the ensuing chapters are provided here.

Grip Stabilization of Novel Objects using Slip Prediction

We propose a grip stabilization approach for novel objects based on slip prediction. Using tactile information, such as applied pressure and fingertip deformation, our approach predicts the emergence of slip and modulates the contact forces accordingly. We formulate a supervised-learning problem to predict the future occurrence of slip from high-dimensional tactile information provided by a BioTac sensor. This slip mapping generalizes across objects, including objects absent during training. We evaluate how different input features, slip prediction time horizons, and available tactile information channels, impact prediction accuracy. By mounting the sensor on a PA-10 robotic arm, we show that employing prediction in a controller's feedback loop

yields an object grip stabilization controller that can successfully stabilize multiple, previously unknown objects by counteracting slip events.

In-Hand Object Stabilization by Independent Tactile Feedback Control

We propose a modular method based on an hypothesis invoked to explain how humans achieve grasp stability. In this biomimetic approach, independent tactile grip stabilization controllers ensure that slip does not occur locally at the engaged robot fingers. These local slips are predicted from the tactile signals of each fingertip sensor (BioTac). We show that stable grasps that are resistant to external perturbations emerge without any form of central communication when such independent controllers are engaged in the control of multi-digit robotic hands for stabilizing a large variety of objects.

Hierarchical Control Decomposition of Dexterous In-Hand Manipulation Tasks

We propose a hierarchical control approach where a higher level policy is learned through reinforcement learning, while low level controllers ensure grip stability throughout the manipulation action. The low level controllers are independent grip stabilization controllers based on tactile feedback. The independent controllers provide the reinforcement learning with a structured exploration of the manipulation task. We show that this structure allows learning the unconstrained task with RL methods that cannot learn it in a non-hierarchical setting. The low level controllers also provide an abstraction to the tactile sensors input, potentially allowing transfer to real robot platforms. We show preliminary results of the transfer of policies trained in simulation to the real robot hand.

1.2 Thesis Outline

This thesis was written such that each chapter can be read independently. However, each subsequent chapter utilizes the findings of the previous chapter in some form. Thus the reader is recommended to follow the outlined order of the chapters to ensure that the connection between each of the chapters is understood. When combined, the chapters guide the reader through a pipeline that attempts to solve the complete dexterous manipulation problem. Beginning with the extraction of relevant information from tactile data in Chapter 2, it is shown how the information provided by state of the art tactile sensors can help robots keep objects stable using a single finger. Once a single finger can stabilize objects with the aid of external surfaces, the natural progression is to attempt to stabilize objects between multiple fingers while keeping the control problem as simple as possible. In Chapter 3 we introduce an approach that does exactly that, by exploring results from neurophysiological studies that suggest that humans solve the problem in a distributed manner. Having the object successfully stabilized between multiple fingers, what remains is to be able to move each of the fingers such that the object displays the desired movements. Chapter 4 shows how to take advantage of the previous distributed control solution in order to not only learn

how to manipulate objects but also to be able do it in simulated environments and directly transfer the learned controllers to real systems.

Chapter 2 shows how to efficiently extract slip information from multi-modal high dimensional tactile signals by autonomously selecting the relevant information from each modality. The extracted signals are used to maintain stable grips between the finger and an external surface by avoiding the occurrence of slip between the finger and the object.

Chapter 3 shows how to scale the grip stability problem to multi-fingered scenarios without scaling the control complexity. To this end, an hypothesis originating from neurophysiological studies of human grip control suggesting that independent and distributed control is able to solve the multi-finger grip stability problem is deployed and validated on robotic systems.

Chapter 4 utilizes the independent distributed controllers proposed in Chapter 3 as the base of a hierarchical control framework. The higher-level controller relies on the lower-level controllers not only to stabilize the object during manipulation actions but also to provide an abstraction between real and simulated environments. This allows the higher-level controller to be learn solely with simulated environment interactions while being able to perform in real environments.

2 Grip Stabilization of Novel Objects using Slip Prediction

2.1 Introduction

Grasping and in-hand manipulation remain challenging tasks in robotics due to a variety of issues. For grasping, it is necessary to infer finger positions on the object and manage the force distribution onto multiple fingers while ensuring grip stability in the presence of uncertainty [5, 7, 4]. Manipulation additionally deals with the contact dynamics between objects and fingers while executing desired motions [96]. For many of these issues, the key problem is how to adapt robot actions in order to deal with undesired contact changes. Controlling the contact state based on meaningful feedback signals may provide a solution to this problem that can potentially generalize across a variety of objects. Here, tactile feedback is an attractive option, as it provides high frequency information directly from the interaction points. Modern, deformable tactile sensors such as the BioTac [90], offer many different measured quantities (e.g., pressure, high frequency vibrations, and temperature fluctuations) while interacting safely due to their compliance. These rich measurements of the local interactions allow the robot to predict the effects of its actions and to adapt them in order to reach the desired contact state. For example, while object stabilization is classically achieved by applying grasps that maximize measures such as form or force closure, we could alternatively accomplish the same goal by minimizing the predicted slip during grasp execution. The classical approach relies on rather accurate contact models, while the slip control method can be based only upon sensory input and prior experience.

Slip, i.e., the partial loss of contact between finger and held object [96], is known to be a key element of human manipulation [41] and may provide robots with the necessary feedback for maintaining grip stability during manipulation actions [84]. For example, such feedback can be used by a robot to reposition objects in its hand through controlled sliding [7]. In robotics, slip can be detected not only from tactile information [59, 36, 83, 77, 34, 72, 37, 84, 13, 29, 35, 81, 24, 1], but also from vision [38], force-torque sensors [88], and laser-based range sensors [58]. Despite the extensive work, approaches based on the sense of touch either rely on large sensors [77, 35], are based on physical models of contact [59, 1], do not use slip information for control [84, 39], or do not evaluate the generalization capabilities of their approach [79, 72]. Further, the mere occurrence of slip is often associated with grasp or manipulation failure. Hence, endowing a robot with the ability *to not just measure slip, but to predict slip ahead of time*, allows it to react prior to the onset of slip. This differs substantially from approaches that focus on sensing actively occurring slip [59, 36, 83, 77, 34, 72, 24, 1] or the closely related problem of detecting

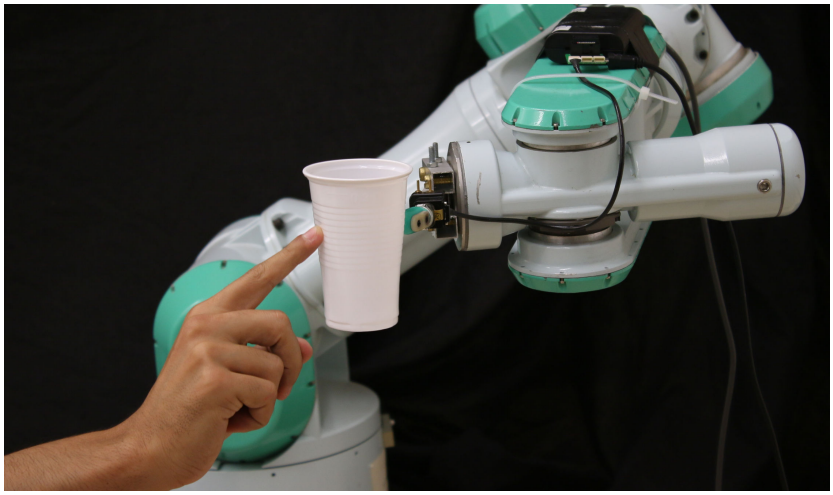

Figure 2.1.: A human-robot grip stabilization experiment where a human and a robot collaborate in order to preserve a stable grip on a deformable plastic cup. A detailed description of the experiment can be found in Section 2.3.7. Results show that the robot is able to respond to actions taken by the human in order to keep the object from slipping. The experimental results are discussed in Section 2.4.6.

the onset of slip, i.e., incipient slip [37, 84, 13, 29, 35, 81, 93]. Correlating the occurrence of slip with object stabilization failure, has the advantage of allowing a grip stability problem to be formalized as a slip avoidance problem. Unlike traditional approaches to grip stability analysis where the entire hand configuration is taken into account [3, 21, 55, 52, 73], avoiding slip takes a more local view, where the stability of the contact surface is assessed.

As a step towards robust in-hand manipulation, we focus on controlling the contact state using a tactile based prediction of slip. From the tactile information provided by the BioTac [90], we learn slip detectors and slip predictors from sampled data (Section 2.2.1). In contrast to other work where the Biotac was used [34, 81], we explore the sensors multiple information channels and autonomously extract the relevant information from each channel. This autonomous extraction of data allows for slip detection/prediction that is generalizable to previously unobserved objects. A similar approach is used in [72] only for detecting slip and with no analysis of generalization performance. Compared to physical modeling and analysis of slip, our approach does not require explicit knowledge on the friction properties or shape of the object.

We incorporate our learned slip detectors and predictors into a feedback controller to perform grip stabilization (Section 2.2) in two scenarios where objects are pinned by a single finger, either jointly with a human as illustrated in Figure 2.1 or against a table as illustrated in Figure 2.2. We compare slip detection to slip prediction and show that stabilizing controllers based on prediction achieve better stabilization performance (Section 3.3). The training is performed using common household objects, where the robot collects labeled data by either pinning the objects or sliding on their surface. We evaluate the generalization capabilities of our controllers by purposely leaving the test object data out of the object data set that is used for training the slip predictors.

This chapter extends our preliminary research results published in [87]. Here, we collect higher time-resolution data, where we autonomously label slip based on fingertip position and applied force. We examine a wider set of feature functions, analyze how each BioTac channel influences slip prediction accuracy and extend the robotic experiments to give further insights into the impact of slip prediction in stabilization control tasks and how well it generalizes to unknown objects.

2.2 Grip Stabilization Control through Tactile-based Slip Prediction

This section gives an overview of our approach to stabilize the grip on objects by predicting slip events. Our approach begins by extracting slip prediction signals from high dimensional tactile data, provided by the BioTac [90]. We formalize the slip prediction problem as a supervised classification problem in Section 2.2.1. Section 2.2.2 then describe the tactile data provided by the sensor and Section 2.2.3 details the tactile features we use as input for prediction. We give an overview of the classification methods used in Section 2.2.4, and describe the controller used for collecting the training data in Section 2.2.5.
Following our learning approach to predict slip, we describe a controller that takes advantage of the prediction signals in order to stabilize grips on multiple objects in Section 2.2.6. This includes objects that are not used in training the slip predictors. The controller attempts to avoid slip events by increasing the contact normal force in response to predicted slip. This control concept has been previously applied in other controllers [77, 35, 72, 81], however, only slip detection was used without prediction of future slip events. Additionally these methods either used much larger tactile sensors or did not analyze the generalization properties of the controller across objects.

2.2.1 Learning to Predict Tactile Slip

In previous work [87], we showed that it is possible to detect and predict slip based on rich tactile signals provided by a highly deformable fingertip sensor. Here, we thoroughly analyze the generalization properties of the best performing approach in [87] while maintaining the problem formalization as a supervised learning problem. Our formalization involves learning a classifier, $f(\cdot)$, that labels the state at time $t+\tau_f$ as slip or not slip,

$$c_{t+\tau_f} = f(\phi(\mathbf{x}_{1:t})), \tag{2.1}$$

where $c_{t+\tau_f} \in \{\text{slip}, \neg\text{slip}\}$ is the state class at time $t+\tau_f$ with t being the current time. The prediction horizon $\tau_f \geq 0$ specifies the future time step in which the predictor is assessing slip. In the case where $\tau_f = 0$, $f(\cdot)$ becomes a slip detector. The feature function, $\phi(\cdot)$, applies a transformation on the raw sensor data, $\mathbf{x}_{1:t}$, providing the input for the classifier. We provide a detailed description of the feature functions explored in this work in Section 2.2.3.

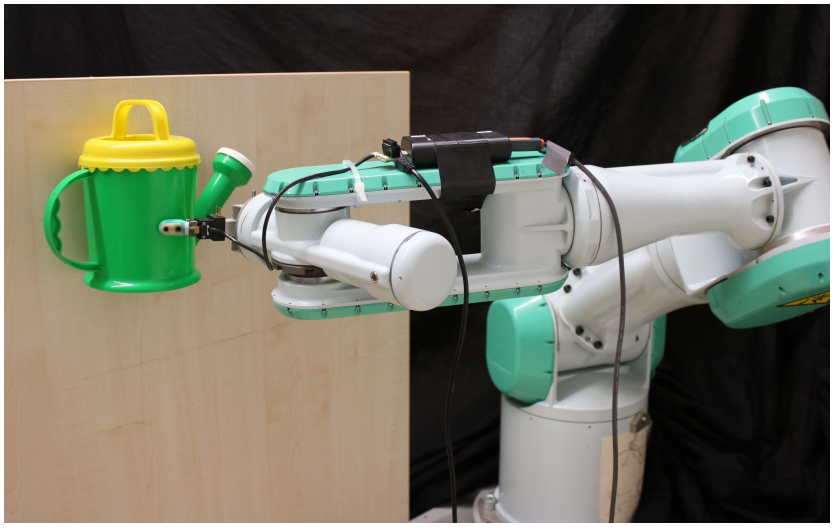

Figure 2.2.: The experimental setup used for our robot in the grip stabilization experiments. We use a Mitsubishi PA-10 robot arm with seven degrees of freedom and a BioTac tactile sensor mounted on the arm as a single finger end effector.

Using this learning formulation, our approach is able to predict slip prior to its onset. As we integrate these signals into the feedback loop of the grip stabilization controller described in Section 2.2.6, we assess how the prediction window size, $\tau_f > 0$, impacts the outcome of the stabilization control, emphasizing the comparison between prediction and detection (i.e. $\tau_f = 0$).

2.2.2 Tactile Sensor Data

The raw tactile data is extracted from the BioTac [90], a multi-channel tactile sensor whose design was inspired by the human fingertip. The sensor is comprised of a rigid core, enveloped by a deformable skin. The space between the core and the skin houses fluid, contributing to the skin's deformability whenever pressure is applied. Inside, 19 impedance-sensing electrodes, distributed across the core's surface, measure the local skin deformation, while a pressure transducer measures fluid pressure and a set of heaters coupled with a thermistor manage and measure the fluid temperature. The sensor output is composed of the electrode signals $E \in \mathbb{R}^{19}$, low frequency, $P_{\text{dc}} \in \mathbb{R}$, and high frequency, $P_{\text{ac}} \in \mathbb{R}$, pressure measurements, temperature $T_{\text{dc}} \in \mathbb{R}$, and temperature flow $T_{\text{ac}} \in \mathbb{R}$. All channels are sampled at a rate of 100 Hz. The P_{ac} is acquired by the sensor at a rate of 2.2 kHz, but is still sampled at 100 Hz, producing batches of 22 values every 10 ms. The resulting sensor state $\mathbf{x}_t \in \mathbb{R}^{44}$, is given by

$$\mathbf{x}_t = [E^T, P_{\text{ac}}^{(1)}, \ldots, P_{\text{ac}}^{(22)}, P_{\text{dc}}, T_{\text{dc}}, T_{\text{ac}}]^T. \tag{2.2}$$

An example of the raw signals produced by the sensor in one of our data collection trials can be seen in Figure 2.3.

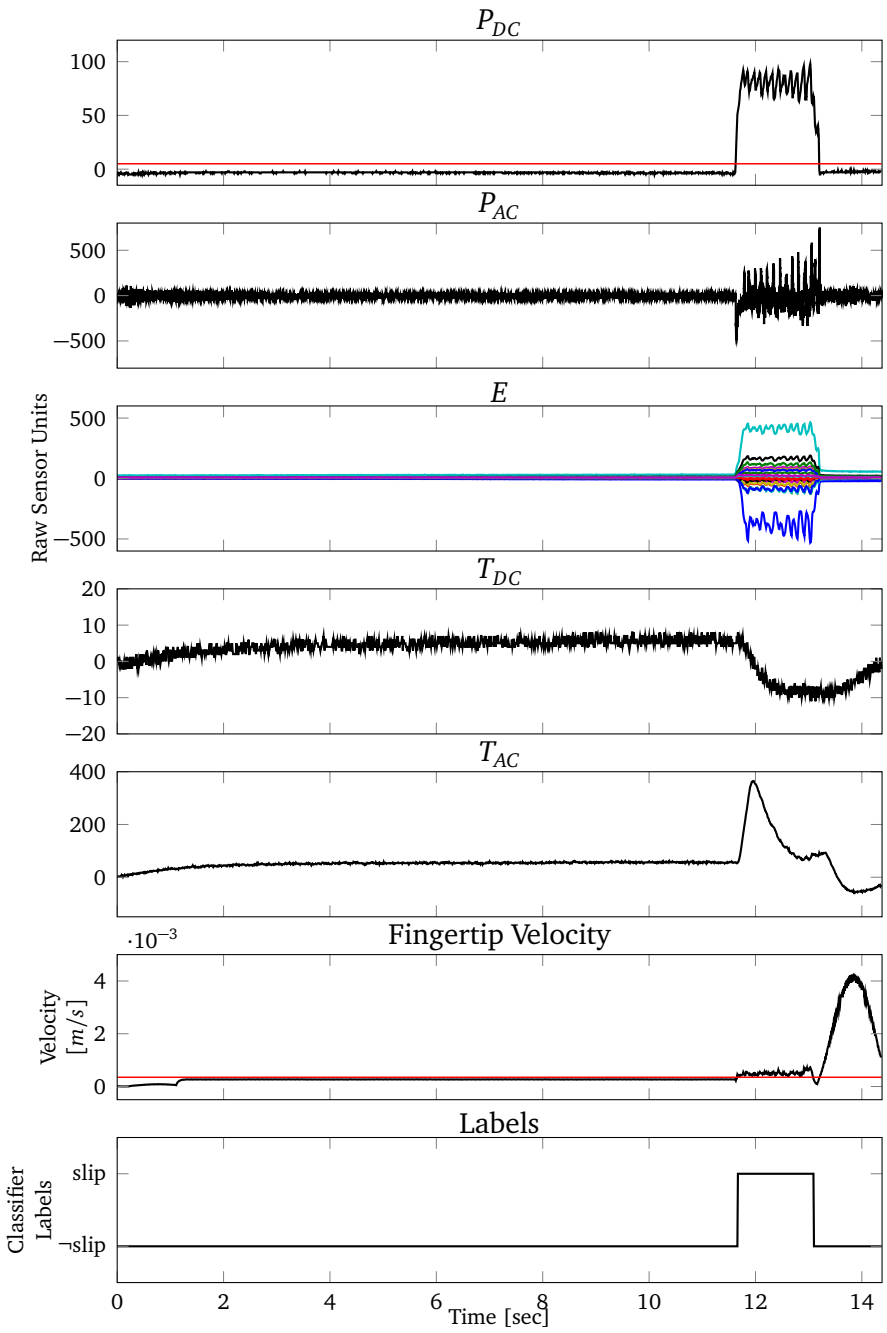

Figure 2.3.: Data traces for one of the data collection trials performed on the ball object. The data collection procedure is described in Section 2.3.2. From top to bottom, we show the low-frequency pressure variations, P_{dc}, high frequency pressure variations, P_{ac}, electrode responses in the fingertip, E, temperature, T_{dc}, temperature flow, T_{ac}, fingertip velocity, and ground truth labels. Sensor values are expressed in raw sensor units with no direct physical meaning. For a detailed description of each sensor channel output refer to [26]. The pressure and velocity thresholds used in the autonomous labeling procedure in Section 2.3.2 are shown in the respective plots.

2.2.3 Tactile-based Feature Functions

We explore several feature functions $\phi(\cdot)$, each of them representing distinct assumptions about the predictability of $c_{t+\tau_f}$ from the accumulation of tactile information over time. If we assume the class label to be directly observable from the current sensor reading $\mathbf{x}_t$,

$$\phi(\mathbf{x}_{1:t}) = \mathbf{x}_t, \tag{2.3}$$

represents the single element feature function. Incorporating the change in the sensor values from the previous time step $\Delta\mathbf{x}_t = \mathbf{x}_t - \mathbf{x}_{t-1}$, yields the delta feature function

$$\phi(\mathbf{x}_{1:t}) = \begin{bmatrix} \mathbf{x}_t \\ \Delta\mathbf{x}_t \end{bmatrix}. \tag{2.4}$$

While the feature functions above only use values directly acquired from the sensor, we consider two complimentary functions that perform frequency analysis on the P_{ac} component, using the extracted properties as features. Based on one of the features proposed by Chu et al. [16], we start by calculating the energy spectral density (ESD), of the P_{ac} signal. The statistics computed on the ESD are the total energy Ω_{s}, spectral centroid C_{s}, variance σ_{s}, skewness S_{s}, and kurtosis K_{s}. We refer to the original work [16] for a more detailed explanation of the feature extraction method. These statistics provide an overview of the time series information given by the P_{ac} channel, no longer viewing the time series values as independent features. The statistics are concatenated with the remainder of the BioTac channels, $\mathbf{x}_t \in \mathbb{R}^{27}$, to produce the complex single element feature

$$\phi(\mathbf{x}_{1:t}) = \mathbf{x}_t = [E, P_{\text{dc}}, T_{\text{dc}}, T_{\text{ac}}, \Omega_{\text{s}}, C_{\text{s}}, \sigma_{\text{s}}, S_{\text{s}}, K_{\text{s}}]. \tag{2.5}$$

As for the single element feature, we also assess how previous time step information can be incorporated in the complex single element feature by setting

$$\phi(\mathbf{x}_{1:t}) = \begin{bmatrix} \mathbf{x}_t \\ \Delta\mathbf{x}_t \end{bmatrix}. \tag{2.6}$$

The resulting feature denotes a complex delta feature.
A second set of features is based on the assumption that $c_{t+\tau_f}$ depends on past sensor readings leading to the current time step t. Multiple feature functions are represented through

$$\phi_\eta(\mathbf{x}_{1:t}) = \mathbf{x}_{t-\eta:t} \tag{2.7}$$

where η controls the size of the window of past data to be considered in each feature function. All sensor readings over the last η time steps are accumulated into an input buffer that is then evaluated by the slip predictor. These features are denoted as the time window η feature functions.
Finally, we also show results when using all features introduced by Chu et al. [16]. By comparing to features that were originally designed with the goal of object prop-

erty learning, we showcase the importance of having the relevant information for predicting slip directly extracted from the raw data by the classifiers.

2.2.4 Classification Methods

To implement our slip predictors, we use random forest classifiers [18], support vector machines [8], and a spectral slip classifier adapted from [27] solely based on high frequency pressure information. In our previous work [87], we show that random forests generally outperform SVMs for predicting tactile slip. As such our analysis mostly focuses on prediction using random forest classifiers.

Random forest classifiers are ensembles of randomly trained binary decision tree classifiers [18]. Each decision tree classifies a given test example independently. The result of the entire forest is obtained by averaging over the distributions of the leaves reached in each of the trees. The class with the highest probability is then selected as the corresponding class for the current sample. Each decision tree is a binary tree where all non-terminal nodes have an associated splitting function, which decides if the currently evaluated example should traverse down the tree following the left or right branch. Leaf nodes contain a probability distribution over the class labels of training examples which reach this node. Tree training consists of selecting the feature and threshold to split at each node. These values are selected through the optimization of a specific performance criterion.

Support vector machines (SVM) are discriminate classifiers that separate the training samples by partitioning the feature space using a single decision boundary [8]. Each partition of the feature space defined by the decision boundary represents a single class. The decision boundary is chosen with respect to the closest samples of each class referred to as support vectors. During training the decision function which maximizes the classification margin, defined as the sum over the distances to each support vector, is found. The resulting linear classifier evaluating feature vector $\mathbf{z}$ takes the form

$$f(\mathbf{z}) = \sum_{i=1}^{k} \alpha_i (\mathbf{z}^T \mathbf{z}_i) + b, \tag{2.8}$$

where α_i is the weight associated with the i^{th} support vector, $\mathbf{z}_i$, and b is a constant offset term. The support vectors and weights can be found efficiently by using quadratic programming. Both implementations of the previous classifiers come from the scikit-learn library for Python [66].

The spectral slip classifier, adapted from [27], computes the total energy in the P_{ac} channel at each time step, after bandpass filtering the output from 30 to 200 Hz. This frequency cutoff band is specifically tailored for the BioTac, as shown in [27]. If the signal energy in this specific frequency band exceeds a threshold Ω_{thresh}, the classifier signals a slip event. We choose Ω_{thresh} by optimizing the classifiers performance over the training data.

2.2.5 Surface Surveying Control for Slip Data Acquisition

In order to train our slip predictors, we require tactile data that has been labeled for slip classification. To collect such data, we perform exploratory actions along the surface of several objects. These actions are two-dimensional trajectories specified on the plane tangential to the contact point with the object and allow the robot to survey the objects surface in multiple directions, creating several different slip examples.

As the object surface is often not planar, a controller is used to ensure that the surveying trajectories are projected onto the object surface. This controller is a hybrid pressure-velocity controller that estimates the corrections that need to be applied to the predefined velocity trajectories, in order to keep the P_{dc} values of the sensor constant throughout the trajectory. Since the P_{dc} value is one dimensional, these corrections are projected onto the contact normal direction that is estimated using the electrode sensors of the BioTac, as proposed by Wettels et al. [92]. The estimate is obtained from the weighted average of the electrodes spatial normals, where the weights are the responses of each electrode. The magnitude of the resulting estimated vector is normalized, resulting in a unit vector in the direction of the applied contact force. To control the P_{dc} values, we calculate the pressure error

$$P_{\text{e}} = P_{\text{dc}}^{D} - P_{\text{dc}}, \tag{2.9}$$

where P_{dc}^{D} is the desired pressure and P_{dc} is the observed pressure. A PD controller is used to regulate the pressure error P_{e} by applying the necessary corrections to the predefined velocity trajectory

$$\mathbf{v} = \mathbf{v}_{\text{des}} + \mathbf{N}(K_p P_{\text{e}} + K_d \dot{P}_{\text{e}}), \tag{2.10}$$

where $\mathbf{v}_{\text{des}}$ is the desired surveying velocity, $\mathbf{N}$ is a unit vector representing the contact normal direction, K_p and K_d are the PD controller gains and $\mathbf{v}$ is the applied task space velocity. The task space velocity $\mathbf{v}$ is integrated in order to acquire the desired task space position and the respective desired joint positions using the robot's inverse kinematics. The surveying controller runs at 100 Hz which is the P_{dc} sampling frequency of the BioTac. The procedure in which the controller is used as well as the survey velocities and desired pressures are discussed in detail in Section 2.3.2.

2.2.6 Grip Stabilization Control using Slip Prediction

Taking advantage of the slip prediction, we design a highly reactive controller that avoids slip regardless of what object it is stabilizing. When slip is predicted to occur, the controller increases the desired task space velocity in the contact normal direction until the robot no longer predicts slip. By adjusting the desired velocity in the contact normal direction, the robot implicitly corrects the applied normal force. If we use the Coulomb friction model for contact, the implicit force adjustment ensures that the applied force remains within the friction cone of the contact location.

Figure 2.4.: The objects comprising our data set. We selected objects covering a range of shapes and stiffness in order to adequately test classifier generalization. In the back we show a tape, followed by a row with, from left to right, a watering can, a box, a cup and a ball. In front we have a standard marker and behind it a measuring stick.

The stabilization control is triggered when the sensor touches the object since we can easily detect contact using thresholds on the sensor pressure values. The predictors run at 100 Hz classifying each sensor state as slip or ¬slip. If the state is labeled as slip, the controller, which also runs at 100 Hz, imposes a desired task space velocity $\mathbf{v}_N(t)$ in the contact normal direction. If the robot predicts no slip, the desired velocity is set to zero. The imposed velocity $\mathbf{v}_N(t)$, corresponds to the contact normal $N(t)$ at time t weighted by a constant δ, i.e,

$$\mathbf{v}(t+1) = \begin{cases} \delta N(t), & \text{if } c_{t+\tau_f} = \text{slip} \\ 0, & \text{otherwise} \end{cases}, \tag{2.11}$$

where δ is empirically defined based on a set of calibration trials where several objects of different weight were tested. The contact normal N is estimated using the method proposed by Wettels et al. [92], described in Section 2.2.5. The controller runs at 100 Hz, reacting to each prediction given by the classifiers.
It is important to notice that the controller does not keep track of the total applied normal force F_N, as it simply increases the velocity in the contact normal direction. As we show, even such a simple controller can perform well when using rich feedback, such as that provided by our slip classifiers.

2.3 Experimental Procedure

In this section, we describe the experimental procedures necessary to realize and evaluate our slip prediction based grip stabilization controller on a real robot. After a short description of our hardware setup in Section 2.3.1, we describe how the sur-

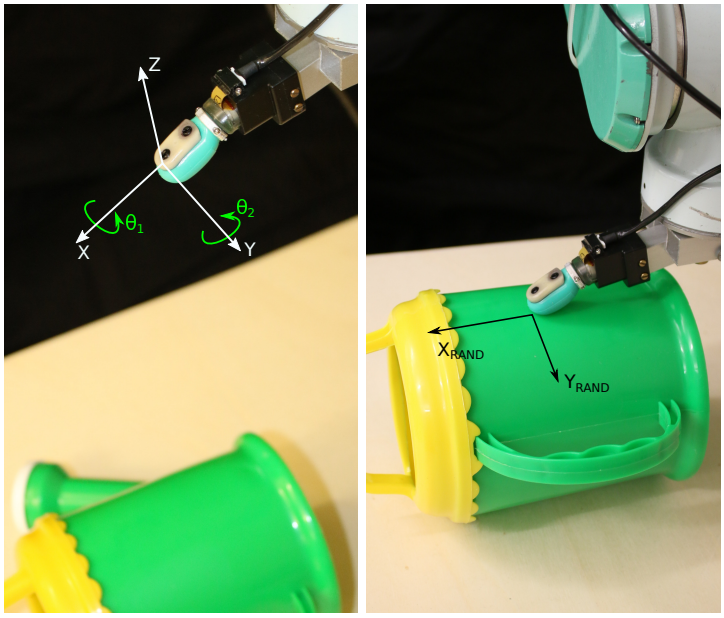

(a) (b)

Figure 2.5.: The random components in the data collection procedure. In (a), two random rotations are applied on the initial position before the finger is lowered to establish contact with the object. In (b), the velocities along the two axes defining the tangential contact plane, are randomly chosen determining the surveying trajectory on the object surface.

face surveying controller from Section 2.2.5 is used to collect the necessary data for training the predictors. The procedure, as well as the number of data collection trials, desired surveying velocities and desired pressures are all discussed in Section 2.3.2. Once the data has been acquired, it needs to be labeled and partitioned into training and test sets. This process is described in Section 2.3.3. With the data labeled, we can finally train the slip predictors. Training is done using three different strategies described in Section 2.3.4, for evaluating the effectiveness of the predictions when a single object, all objects, or all objects excluding the test object are used.
As our data set is unbalanced in the number slip examples, versus the number of ¬slip examples, we evaluate the predictors with the F_{score} metric. In Section 2.3.5, we describe and motivate the use of this metric in our analysis.
Finally, to evaluate the performance of the grip stabilization controller, we perform two sets of experiments. In the first set of experiments, described in Section 2.3.6, the robot stabilizes the gripped object between the finger and a fixed plane, evaluating the success rate of the stabilizations. The second set showcases the robustness of the stabilization by having the robot stabilize an object gripped jointly with a human experimenter. We describe this more dynamic experiment in Section 2.3.7.

2.3.1 Robotic Platform

All robotic experiments described in the following sections were performed using a Mitsubishi PA-10, a robotic arm with seven degrees of freedom. A BioTac tactile sen-

sor, described in Section 2.2.2, was rigidly mounted to the arm as a single finger for manipulation. We directly control the arm's joint positions at a frequency of 100 Hz. The complete experimental setup can be seen in Figure 2.2.

2.3.2 Slip Data Collection Procedure

We acquired the data used to train our slip classifiers through two separate procedures specifically designed for collecting examples for slip states and static contact states.
In the slip procedure, the object was fixed to a table. The robot first moved to an initial position above the object. Two random rotations were applied to the initial position in each trial as shown in Figure 2.5a, ensuring different initial contact locations between the fingertip and the object across trials. Following the random rotations, the robot moved the fingertip down toward the object until achieving contact and a desired pressure P_{dc} was reached. Thereafter, a random velocity vector was defined in the plane tangential to the contact point as shown in Figure 2.5b. This velocity is denoted by $\mathbf{v}_{\text{des}}$ in the surface surveying controller in Equation (2.10) and never exceeds 0.05 m/s. After performing the movement along the object's surface, the robot returned to its initial position. Each procedure was repeated ten times for each of the seven objects for three different target pressure values, making a total of 30 trials per object.

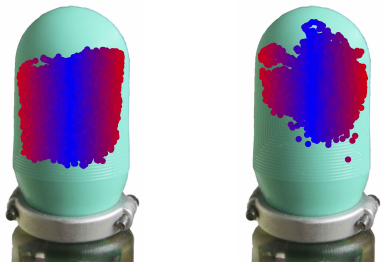

(a) (b)

Figure 2.6.: Estimated contact locations on the fingertip sensor during (a) data collection and (b) the stabilization against a fixed plane. The points at the center of the BioTac are displayed in blue while peripheral contacts become progressively red as the distance to the center increases.

For the static contact data collection, the procedure was similar. The difference was that after the robot moved down and contact was established, there was no longer movement along the tangential contact plane. The robot effectively stays in static contact with the object for one second in each of the trials. This procedure was also repeated ten times for three target pressure values resulting in another 30 trials for each of the seven objects. With both procedures combined, 60 data collection trials were performed per object for a total of 420 trials. The target values for P_{dc} used in the experiments were 20, 50, and 80. All sensor values were considered with respect to sensor baselines collected at a resting posture (no contact). The random components introduced in the rotation of the initial position and the magnitude of the tangential surveying velocity, serve to cope with the multiple locations and velocities in which slip may occur on the fingertip. Figure 2.6 shows how finger contact locations collected during training compare to those produced during grip stabilization experiments performed on the robot. These stabilization experiments are described in detail in Sections 2.3.6 and 2.3.7.

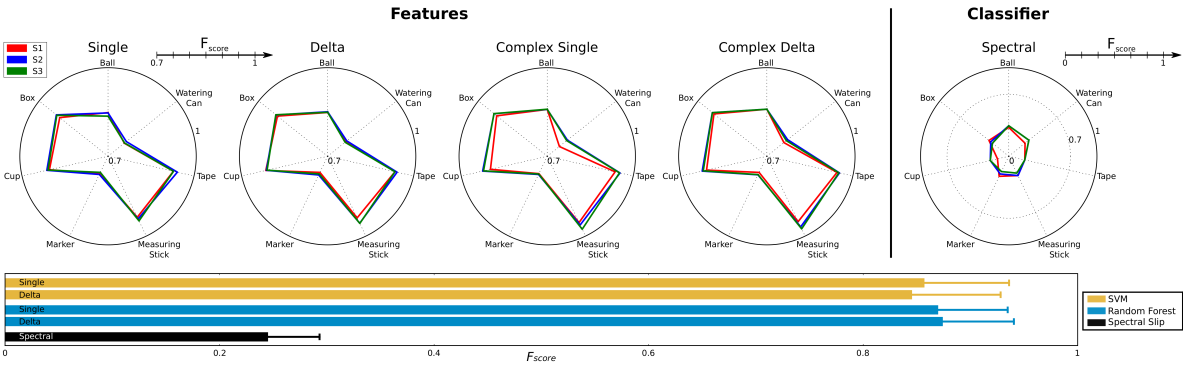

Figure 2.7.: Slip detection results showing (top) F_{score} achieved by random forest and spectral detectors for each feature and (bottom) mean and standard deviation across all objects for each of the classifiers. Plots for the individual features show results for each object, comparing across training strategies (single object $S1$, all objects $S2$ and leave one out $S3$) introduced in Section 2.3.4. The F_{score} for the proposed features shows similar patterns across all objects and all strategies. Note that the F_{score} minimum for the spectral slip radial plot is zero in contrast to 0.7 in the remaining plots. This is highlighted in the mean plots, where the random forests and spectral detectors respectively show the best and worst performances.

2.3.3 Data Labeling and Partitioning for Training and Testing

Before the collected data can be used, it needs to be properly labeled. The labeling process was performed autonomously, relying on the robot's forward kinematics and the overall pressure on the fingertip. In a first stage, we removed data according to a contact threshold, P_{thresh}, on the P_{dc} values. If the finger pressure was below P_{thresh}, the finger was considered not in contact with the surrounding environment, and the corresponding time step was removed from the training data. The remaining data was then labeled as slip or static contact using a threshold, Δq_{thresh}, on the instantaneous end-effector velocity, Δq, estimated by calculating the difference in end-effector position between two consecutive time steps. If Δq was greater than Δq_{thresh}, the finger position was changing with respect to the object while contact was established and the data was labeled as slip. If Δq did not exceed the threshold the data was then labeled as static contact. Both thresholds P_{thresh} and Δq_{thresh} were tuned by an expert by observing the sensor data and the corresponding labels produced by each threshold pair. Increasing P_{thresh} resulted in more data points being removed due to being considered non-contact examples, while larger values of Δq_{thresh} implied that fewer contact examples were labeled as slip. We show the pressure values, instantaneous end-effector velocity, respective thresholds, and resulting labels in Figure 2.3 for one of the trials.

After the data was labeled, trials were partitioned into training and test sets. The training set was used for training the slip classifiers and was composed of seven of the trials for each object and P_{dc} value pairs. The remaining three trials per set were used to validate the classifiers after training. The same training and test sets were used for all experiments.

2.3.4 Training Strategies

We analyze slip detection and prediction according to the accuracy and generalization capabilities of our classifiers by introducing different training strategies. The first strategy ($S1$) involves training the classifiers on a single object and evaluating how they can classify slip on that same object. This strategy is denoted per object training and serves to evaluate how well slip can be classified on an object when only that object is known. Another training strategy, denoted all object training strategy ($S2$), involves using data from all objects during training and assessing the classification performance on each object individually. When making a comparison between these first two strategies, we can effectively assess how slip classification rates for a single object change when multiple objects are known. If an increase in classification rate is observed for any single object when transitioning from $S1$ to $S2$, we can assume that relevant transfer of slip information is occurring between objects. Finally, in order to assess the generalization capabilities of the classifiers, a leave one out training strategy ($S3$) is used. In $S3$, classifiers are trained on data from all objects except one, that is used for testing the generalization to novel objects. If similar classification rates are achieve with $S2$ and $S3$, slip information transfer to between-object cases can be said to compensate for the absence of information regarding previously unobserved objects.

2.3.5 F-Score Metric

After performing the data collection and labeling procedures of Sections 2.3.2 and 2.3.3, we verified that the resulting data set was unbalanced in the number of class examples. Since the surveying motions only represent a small part of each data collection trial, the resulting data set is biased in the number of class samples, i.e., the slip examples are greatly outnumbered by the ¬slip examples.

Evaluating our classifiers based on classification accuracy, we observe very high accuracies (above 90%) from classifiers that simply label everything as ¬slip. Considering it is more important to detect when slip occurs then when it does not, a more helpful analysis of the classification results is performed by reporting the F_{score} instead of classification accuracy. The F_{score} is a harmonic mean of the precision and recall measures

$$F_{\text{score}} = 2\frac{pr}{p+r}. \tag{2.12}$$

The precision, p, depicts the ratio between accurate positive classifications and total positive classifications

$$p = \frac{\text{true positives}}{\text{true positives} + \text{false positives}}. \tag{2.13}$$

In our case, precision evaluates the quality of the classifiers predictions by calculating the ratio of correct slip predictions with respect to the total number of slip predic-

tions made by the classifier. The recall, r, is the ratio between accurate positive classifications and positive examples

$$r = \frac{\text{true positives}}{\text{true positives} + \text{false negatives}}. \tag{2.14}$$

Here, recall represents how likely the classifiers are to miss slip instances by calculating the ratio between all instances where slip was predicted with respect to all instances where slip should have been predicted.

When the predictions are correct (high precision) and few slip instances are missed by the classifier (high recall), the F_{score} approaches its maximum value of one. If the classifier either predicts several instances of slip incorrectly (low precision) or misses several slip instances (low recall), the F_{score} approaches its minimum value of zero.

2.3.6 Stabilizing Objects against a Fixed Plane

Following the evaluation of our slip predictors, we describe the first experiment that showcases the relevance of the acquired slip prediction signals in the context of grip stabilization. The experiment involves stabilizing the grip on an object pinned between the fingertip sensor and a fixed table, as show in Figure 2.2. The grips are performed on unknown objects to test the generalization capabilities of our prediction based stabilizers.

To perform grip stabilization, the previously trained random forest slip predictors are embedded in the feedback loop of the grip stabilization controller presented in Section 2.2.6. The random forests are trained with a leave one out strategy ($S3$), and a number of grip stabilization trials are performed on the object that was left out of the training set. Each trial consists of the robot initially pinning the object against a vertical plane. Once the object has been successfully stabilized against the plane, a random velocity is applied to move the robot away from the object. The three components of the exit velocity are sampled from different Gaussian distributions. The two lateral velocity components are sampled from Gaussian distributions with 0.0 m/s mean and 0.05 m/s standard deviation and the exit component is sampled from a Gaussian distribution with 0.05 m/s mean and 0.05 m/s standard deviation. As the robot moves away from the object, and as soon as slip is predicted, the stabilization controller becomes active, counteracting the exit motion and attempting to re-stabilize the object. The stabilization controller remains active until no slip is predicted during a period of 2 seconds or for a total of 10 seconds, after which the trial finishes. If the robot does not drop the object before the trial concludes, the trial is considered a success. We conduct ten trials per object for each feature function and prediction windows $\tau_f \in \{0, 5, 10, 15, 20\}$ and report the percentage of successful trials for each combination across all objects.

2.3.7 Human-Robot Joint Grip Stabilization

In order to assess the robustness of our slip prediction based grip stabilizers, we attempt to stabilize a grip on an object jointly with a human experimenter, by replacing the vertical plane with one of the experimenter's fingers.
Initially, the experimenter holds the object. As soon as the robot touches the object, the experimenter repositions his hand, and leaves only a single finger in contact with the object, as depicted in Figure 2.1. Simultaneously, the stabilization controller is activated. The experimenter makes a qualitative assessment of the robot's performance as it tries to compensate for his movements. This qualitative assessment is a relative preference between controllers, where each controller uses a different feature for predicting slip. The assessment is based on the responsiveness and stability (oscillations when attempting to keep the object still) of each controller. Note that the grip stabilizers have to cope with the random noise introduced into the system by the experimenter. In addition, a thin plastic cup is used in this experiment. This object is not present in the previous object set, and is completely unknown to the slip predictors. The evaluation was repeated three times for each of the predictors and was performed by a single experimenter.

2.4 Results

In this section we report the results of our evaluation for both the slip predictors and the grip stabilizers based on the predictors outputs. We begin with a brief comparison of results achieved with the different classification methods, Section 2.4.1, in order to confirm our previous findings [87], with the newly acquired data set. The classifier comparison is followed by an analysis of the individual performance of each BioTac channel for slip detection in Section 2.4.2, showcasing the importance of having the classifiers extract the relevant information from each of the BioTac channels. The performance of our slip detection and prediction classifiers as well as the relevance of the proposed features in both cases is reported in Sections 2.4.3 and 2.4.4 respectively. Finally, the success rates achieved for our grip stabilizers in the stabilization against a fixed plane experiment are reported in Section 2.4.5 and the results from the human-robot joint stabilization experiment are reported in Section 2.4.6.

2.4.1 Classifier Comparison

The average over $S1$ and $S2$ is used to compare the three classifiers described in Section 2.2.4. We examine the SVM and the random forests with two of the proposed features and use the P_{ac} signals as input to the spectral slip classifier. From the results shown in the bottom plot of Figure 2.7, we observe that SVM performance is on par with the performance achieved with random forests. The spectral slip classifier performance is much worse than the performance of the other two classifiers.
A more detailed comparison between the best and worst performing classifiers, respectively the random forest and the spectral slip classifiers, is shown on the radial plots of Figure 2.7, and in a comparison between the ground truth labels and the

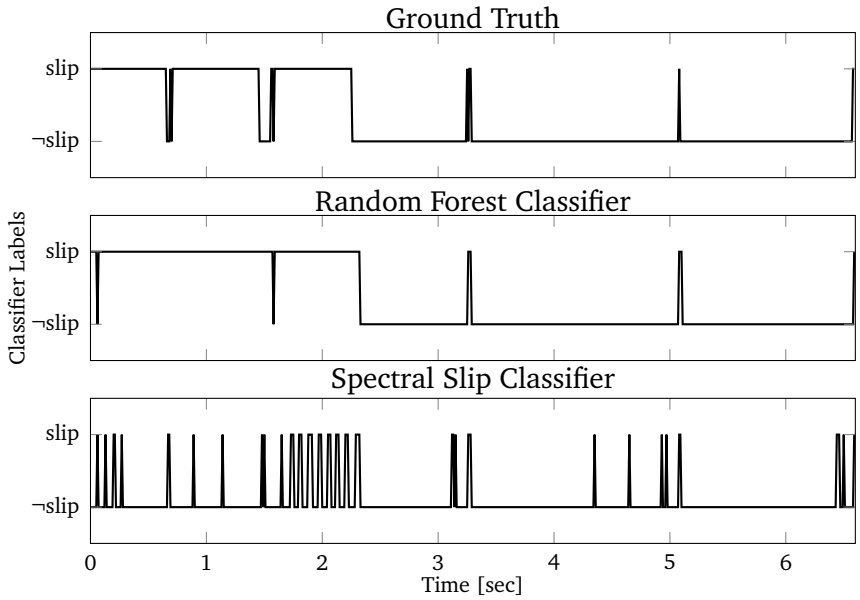

Figure 2.8.: Traces of the ground truth labels and the labels generated by the random forest and spectral slip detectors for one of the test trials. While the random forests very accurately reproduce the ground truth results, the spectral slip classifier is only able to detect the ground truth slip transitions, failing to detect continuous slip.

labels produced by both classifiers in Figure 2.8. The radial plots show similar F_{score} patterns for all training strategies and, in the case of the random forests, across four of the proposed features. From the traces in Figure 2.8, it is clear that the spectral classifiers accurately detect the onset of slip, but fail to continuously label slip as the finger surveys the object's surface. These findings suggest that spectral signals are prone to noise caused by motor induced vibrations during trajectory execution. Using all the BioTac channels, the impact of the noise is reduced, explaining the higher accuracy observed for the SVM and random forest classifiers throughout continuous slip phases. Following these observations, and considering that the random forests slightly outperform SVMs in terms of the mean value, the remaining results to be presented in this chapter are associated with classifiers trained using random forests.

2.4.2 BioTac Channel Relevance Analysis

In order to better understand the contribution of each BioTac channel for the detection of slip, we compare slip detectors that are separately trained with each channel as input using $S2$. The results are shown in Table 2.1. As a reference, results obtained by a slip detector trained with the single element feature are included in the right most column of Table 2.1.

The electrode information dominates the classification performance, achieving the best score on all objects except the marker. The pressure information from P_{ac} and P_{dc} are fairly successful, with the P_{dc} alone achieving the best performance for the marker. Further, the temperature channels, T_{dc} and T_{ac}, provide no meaningful abil-

ity to detect slip. These results show that the deformation information present on the BioTac can be used to detect slip extremely well. This observation is especially relevant as deformation information is not traditionally associated with the detection of slip. Vibration information stored in the P_{ac} and P_{dc} offers good detection rates, while not having an average performance comparable to the electrodes. Finally, results achieved with the single element feature function show that the detectors are able to consolidate information from multiple channels, improving the slip detection rates.

2.4.3 Slip Detection and Feature Influence

From the results shown in the radial plots of Figure 2.7, we see that for four of the proposed features, the random forests can successfully classify slip, although different success rates are observed depending on the object. For objects such as the box, cup, tape and measuring stick, slip is classified quite accurately. On the remaining objects, despite lower classification rates than for previous objects, F_{score} values are still above 0.7. When comparing training strategies, we observe that classification performance remains mostly the same across all strategies, hinting that (1) not much knowledge is gained from additional objects once the target object is already known and (2) the classifiers can generalize quite well for previously unknown objects.

In Figure 2.9, we show results across all features when averaging over $S1$ and $S2$. While the time window η features perform quite well, there is no significant difference in performance with respect to the single element or the delta features. In fact the top performing feature is the complex delta feature. The complex versions of the single element and delta features seem to outperform their simpler counter parts. This suggests that condensing the time series information provided by the P_{ac}, as described in Section 2.2.3, benefits the detection rate. Finally, the features of Chu et al. [16], albeit being the worst performing features, still achieve good detection rates. This is surprising since they were designed with other tasks in mind. In fact these fea-

Table 2.1.: F_{score} for different detectors where each of the BioTac channels is used as the only feature of the classifier. All results are for the random forest classifier trained on all objects ($S2$). Bold values indicate the best F_{score} value obtained per object, excluding results obtained when using detectors trained using the single element feature function.

	E	P_{ac}	P_{dc}	T_{ac}	T_{dc}	$\mathbf{x}_t$
Ball	**0.793**	0.642	0.696	0.161	0.196	0.847
Box	**0.876**	0.683	0.702	0.099	0.184	0.925
Cup	**0.809**	0.614	0.596	0.171	0.072	0.913
Marker	0.718	0.559	**0.802**	0.249	0.003	0.768
Measuring Stick	**0.905**	0.701	0.665	0.099	0.087	0.936
Tape	**0.886**	0.617	0.706	0.088	0.053	0.942
Watering Can	**0.667**	0.637	0.634	0.172	0.402	0.780

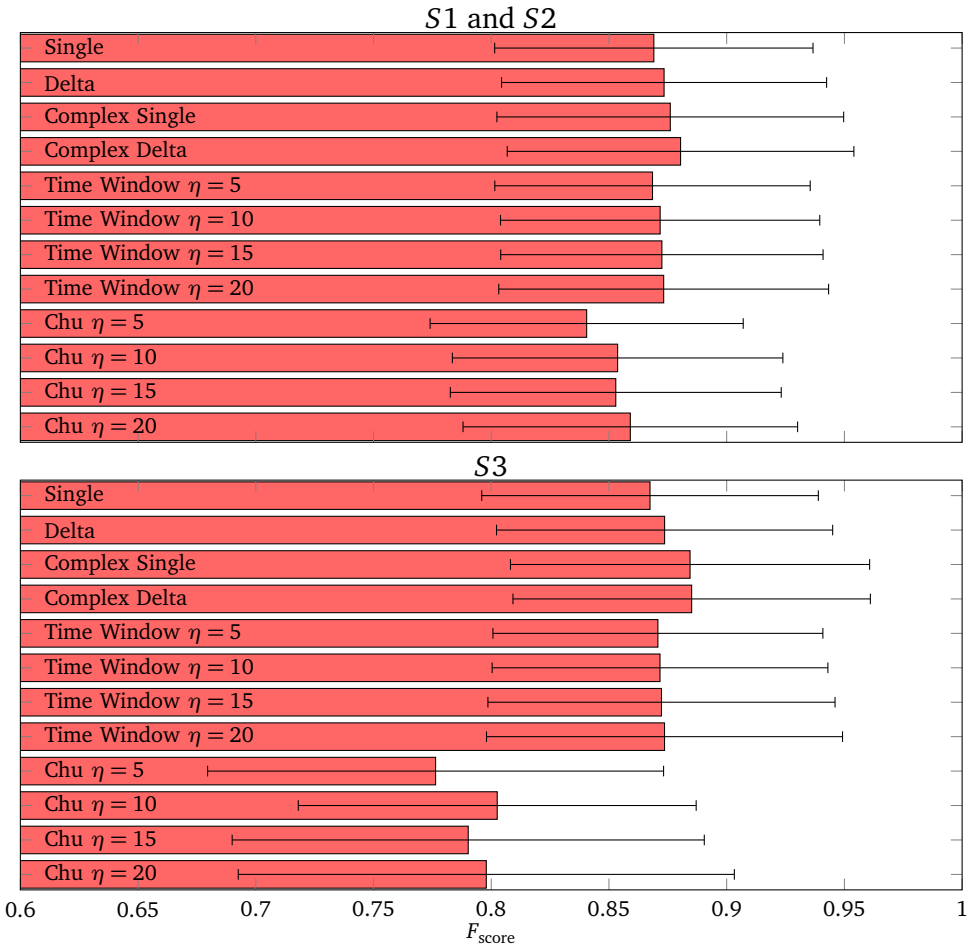

Figure 2.9.: The mean F_{score} and standard deviation obtained per feature for slip detection. These results show the average performance jointly over $S1$ and $S2$ (a) and when only considering $S3$ (b). The memoryless and short term memory features outperform the long term memory features with respect to the mean F_{score}. When testing generalization with $S3$, a significant drop of performance is observed for the features of Chu et al. [16].

tures cluster information over temporal windows which are large in comparison to the duration of slip events.

Figure 2.9 also shows average results over $S3$ for each feature. The same performance patterns are observed as in the previous experiment, with the complex delta feature still as the top performing feature. The features of Chu et al. [16] perform significantly worse than in earlier experiments. This suggests that the information retained by these features is specific to the objects observed and does not generalize well to novel objects. These findings support our choice of having the features built only under data aggregation assumptions, relying on the classification approach to balance the multi-channel information.

Considering the results shown so far and taking into account that we aim for real time performance on the real robot, we base the rest of our analysis on the single element and delta features and their complex counterparts. It is hard to justify the additional computation power required to process the time window η features in real time, as

we do not observe any advantages in terms of classification performance when using these features.

2.4.4 Slip Prediction Offline Results

In this section, we analyze how the classifiers perform when $\tau_f > 0$, by training slip predictors with prediction horizons τ_f of 5, 10, 15, and 20 steps, equating to times of 0.005, 0.01, 0.015, and 0.02 seconds respectively. Following the same type of analysis as performed for slip detection, we observe that there is no significant difference between the results obtained for the average of $S1$ and $S2$ and the results obtained for $S3$, shown in Figure 2.10. We observe similar F_{score} values as with slip detection, clearly showing the feasibility of predicting slip. Nonetheless, a consistent drop in classification rates can be observed for $\tau_f = 15$. A more in-depth analysis reveals that, while prediction rates for most objects remain stable from $\tau_f = 10$ to $\tau_f = 15$, a decrease in rate can be observed for the ball and the watering can when using the single and complex single features. For the delta and complex delta features, a significant performance drop is observed only for the watering can. In terms of best performance, the delta feature overtakes the complex delta feature for $\tau_f \geq 10$. Further, complex features display a more accentuated drop in performance with increasing values of τ_f. This performance drop suggests that, despite having good discriminative and generalization properties, the complex features are not as suited for prediction due to their more compact representation of the P_{ac} signals that results in a loss of relevant information for prediction.
The results show that it is not only possible to predict slip but that it also possible to generalize the prediction of slip to previously unknown objects, producing the desired feedback signals for the controller described in Section 2.2.6.

2.4.5 Grip Stabilizing Control on the Real Robot

In order to assess the performance of our slip based grip stabilizers, Figure 2.11 reports the success rates for the stabilization of objects against a fixed plane experiment, described in Section 2.3.6. Results are show for each object separately, while comparing feature functions and τ_f values. By comparing different values of τ_f, we are assessing how earlier controller responses (larger prediction windows) affect the grip stabilization success rates. We observe an increase in the stabilization rates with τ_f for all objects, specifically for the cases where $\tau_f \geq 10$. Note that the increase in stabilization rate is particularly interesting considering the results shown in the previous section, where prediction accuracy dropped for $\tau_f \geq 10$. Although prediction accuracy is lower for this range of τ_f, the ability to predict farther into the future facilitates the stabilization task.
Spectral slip classifiers perform quite well independently of the value of τ_f and changes to τ_f do not seem to influence the performance of the spectral slip controller. Their performance is unexpectedly high, considering the results obtained in the offline evaluation. Careful observation of the stabilization trials confirms the results obtained in the offline experiments, where spectral slip predictors capture very

accurately the transition from static contact to slip (transition from ¬slip to slip) but only as it is occurring. On the other hand, accurately detecting slip only as it occurs proves insufficient to stabilize all objects. For light objects, the brief response of the controller to the initial slip transition is enough to stabilize the object. This is the case for the ball, box, cup and marker. For objects such as the measuring stick or the watering can, the brief response generated by the controller during this first slip transition is insufficient to fully stabilize the object, as they are heavier and, in the case of the watering can, suffer from larger torsional slips. When comparing the predictors with the spectral slip classifiers, the latter outperform our approach for $\tau_f \leq 10$ but, as τ_f increases, controllers using the predictors eventually achieve the best stabilization rates for objects where previous performance was inferior to that of the spectral slip classifier.

Similar results can be observed in Figure 2.13, where the mean and standard deviation of the grip stabilization success rates across all objects are shown per feature and per value of τ_f. These results clearly show the consistent behavior of the controllers using spectral slip classification, unaffected by changes to the value of τ_f. For controllers relying on our proposed slip predictors, a clear pattern is observed, where stabilization performance increases with τ_f, eventually matching the performance of the spectral slip classifiers or even outperforming it for $\tau_f \geq 10$. In addition, it is also clear that despite the decrease in prediction rates observed for $\tau_f = 15$, there is an

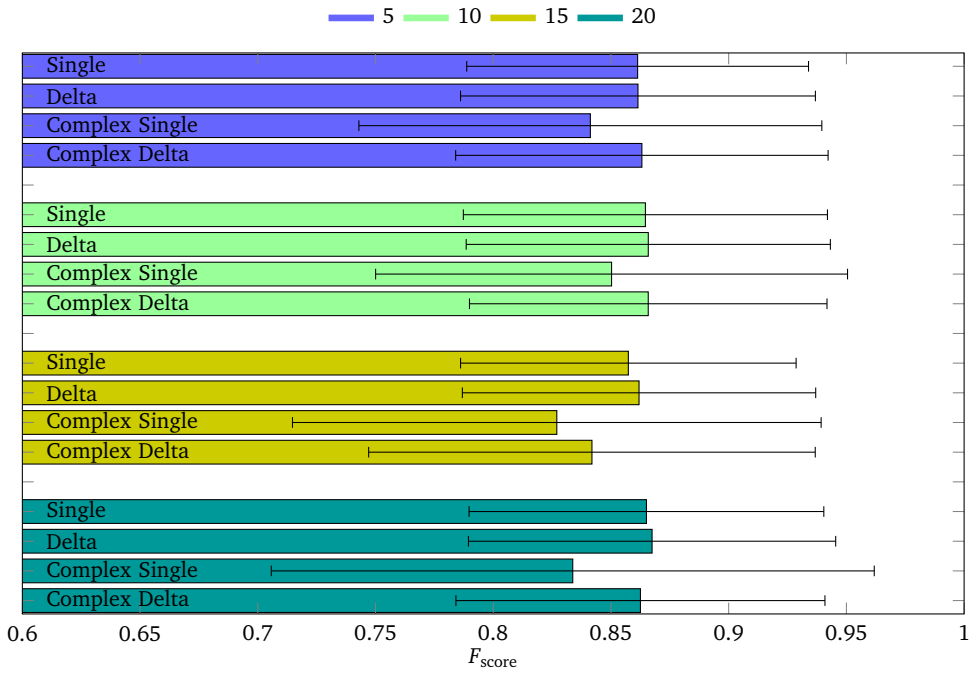

Figure 2.10.: The mean F_{score} and standard deviation obtained per feature for slip prediction with several prediction windows, τ_f. These results show the performance when only considering $S3$, hence testing how slip prediction generalizes to novel objects. While the complex features show better average results for low values of τ_f, the delta features show the top performance for $\tau_f > 10$, suggesting that the complex features are not as suited for prediction.

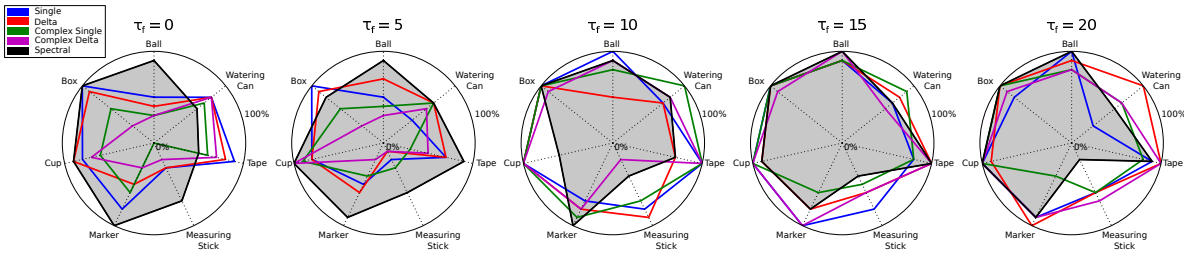

Figure 2.11.: Stabilization success rates of the slip prediction based controllers for each of the objects. The success rate represents the percentage of trials for which the robot successfully stabilized the object. All predictors are trained with a leave one out strategy $S3$. Different values of τ_f are considered results are shown for each feature. The filled region represents the performance of the controllers using the spectral slip classifier. It is clear that the performance of all proposed features increases with τ_f.

increase in stabilization success rate. The exception is the controller using the predictors trained with the complex single feature, which was the feature with the most significant drop in performance for $\tau_f = 15$. This confirms that, on average, the ability to predict slip further into the future has a bigger impact in controller performance than the resulting drop in prediction accuracy due to a larger value of τ_f.
We evaluate if there is a statistically significant difference between the success rates as a function of prediction time horizon. We conduct a separate test for each feature type. We perform a Kruskal-Wallis H-test [47], a non-parametric version of the popular ANOVA test. The Kruskal-Wallis H-test is chosen since the variances of the distributions are not equal, a necessary assumption for the ANOVA test. The results show that there is no statistically significant differences between prediction horizons for the spectral and the single element features, with p-values of 0.9563 and 0.1386 respectively. On the other hand, for the delta, complex single, and complex delta features, there is a statistically significant differences between the distributions, with respective p-values of 0.04688, 0.0029 and 0.0091. For these three features, the results are not surprising, as they display the most accentuated increases in success rate.
Traces for the P_{dc}, fingertip position along the contact normal axis and predictor response are shown for a trial on the watering can using the delta feature with $\tau_f = 20$. After the initial perturbation occurring at 5.4s, whenever slip is predicted to occur, shifts in the negative contact normal direction and increases in the fingertip pressure can be observed. Following the 7.6s mark, the object remains stable for 2s and the trial concludes successfully.

2.4.6 Cooperative Grip Stabilization

By using controllers based on our slip predictors, the robot is able to successfully complete the human-robot joint grip stabilization task. While all controllers were able to jointly stabilize the objects, the experimenter found that as τ_f increased, the controller's response time was shorter, compensating for more sudden movements.

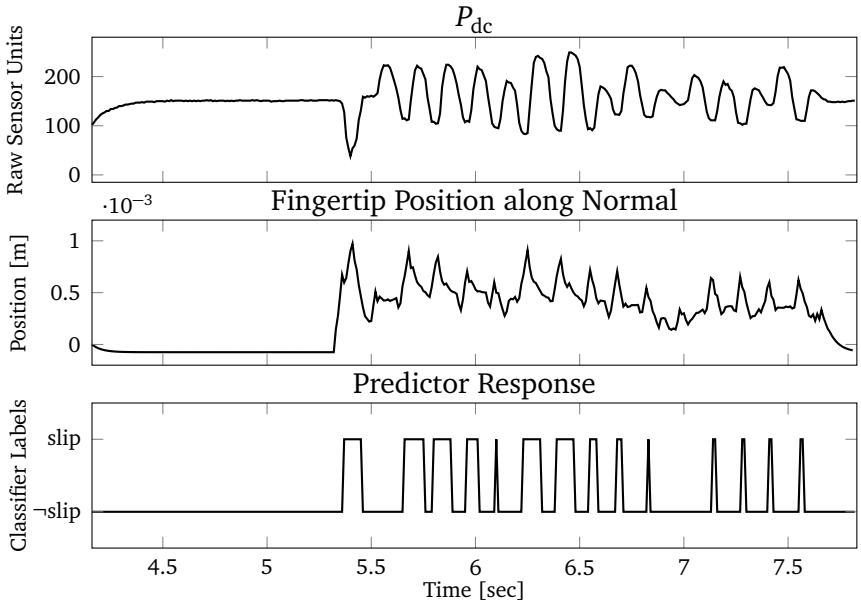

Figure 2.12.: Traces of the P_{dc}, the fingertip position along the contact normal and the predictor responses during a trial of the grip stabilization against a fixed plane experiment. The slip predictor used in this trial was trained with the delta features and a prediction window $\tau_f = 20$. After an initial perturbation, the grip stabilizers adjust the position of the fingertip, moving it towards the table (in the negative direction of the axis) whenever slip is predicted to occur.

The spectral slip method completely failed to stabilize the object with the human. The spectral slip's inability to classify continuous slip causes the controller to react only in short bursts as described in Sec. 2.4.5. For the movements produced by the human, where the duration and velocity of the movement is unknown, these extremely short responses are insufficient to keep the object stable.

To compensate for the accelerations introduced by the human, we replace a constant valued δ with a function $\delta(t)$ that increases linearly with time since slip was detected. The value of $\delta(t)$ returns to zero whenever ¬slip is detected. For small movements, the robot does not apply the maximum response instantly, avoiding crushing the object or injuring the experimenter. As its response varies over time, the robot can cope with longer movements of variable velocity, by constantly readjusting its response.

2.5 Conclusion and Discussion

The proposed slip prediction based grip stabilization controllers were inspired by studies on human manipulation, specifically, neuroscientific studies suggesting that the human tactile system has a strong discrete feedback component, and relies on sensory prediction for control [41].

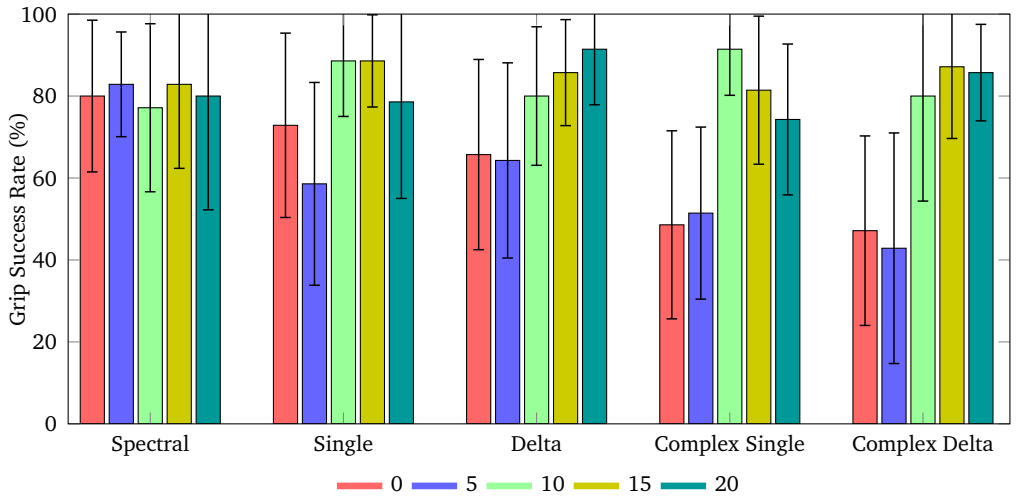

Figure 2.13.: Mean and standard deviation of the success rates for the grip stabilization experiments against a fixed plane experiments on the real robot. The success rate represents the percentage of trials where the robot successfully stabilizes the object, out of a total of 70 trials (10 per object). By varying the prediction window τ_f, we evaluate how the ability to predict slip farther into the future impacts the stabilization success rates of the controllers. While changes to τ_f have no effect on the controller using the spectral classifier, for all other controllers the success rates clearly increase for larger prediction windows.

2.5.1 Summary of the Contribution

In this chapter, we have presented a learning based approach for predicting slip from high dimensional tactile information. Our slip predictors are integrated into the feedback loop of a grip stabilization controller allowing it to compensate for slip before its onset. Controllers based on predicted slip signals are shown to increase stabilization rates when compared to controllers solely relying on the detection of slip. In addition, we show the controllers to be highly generalizable to novel objects and sufficiently robust for the robot to stabilize objects jointly with a human. This robustness to severe perturbations, observed during the human-robot joint grip stabilization experiment, shows that such an approach can potentially be used for multi-fingered cases during in-hand manipulation.

2.5.2 Recognized Shortcomings

The proposed grip stabilization approach aims for the generalization of the slip sensation based control across a wide range of objects. To fulfill such a goal, a diverse training data set is required, in order to cover a broad set of interactions. Such data sets are not readily available, and have to be collected by experts in the field. Additionally, the data has to be labeled for the slip events, requiring highly accurate systems or several man hours to label the data manually. Our approach fails to compensate for rotational slip as the data collection procedures introduced in Sec-

tion 2.3.2 were not designed to collect data for rotational events. Finally, training such methods with the required amounts of data is time consuming and sometimes renders them slow at execution time when compared to simple approaches such as the spectral slip classifier.
The controller proposed in Section 2.2.6 is highly affected by the heuristic used for the estimation of the normal contact direction. This estimation is very noisy and should be improved to solve more complex tasks.

2.5.3 Future Work

Our work has focused on merging multiple tactile sensing modalities for predicting slip and on the usefulness of these predictions for grip stabilization with a single finger. A natural next step is the extension of this approach to multi-fingered manipulation tasks, where we wish to analyze how multiple fingers, each with its own tactile sensor, can be integrated in order to perform in-hand grip stabilization and possibly facilitate in-hand manipulation.
While we chose slip prediction as a first step, we see the possibility of using the proposed learning approach for the prediction of contact breaking (e.g., during a controlled release of an object) as in re-grasping or finger gaiting or for predicting the onset of a lift phase (i.e., when the held object leaves the supporting surface).

3 In-Hand Object Stabilization by Independent Tactile Feedback Control

3.1 Introduction

Robotic grasping and in-hand manipulation are traditionally viewed as monolithic planning and control problems. As such, control policies determine the approach strategy and finger placement (contact forces and contact locations) for the entire hand, while considering finger trajectories, force and contact profiles throughout the entire manipulation task [33]. This monolithic formalization requires accurate kinematic and dynamic models of the hand along with precise sensing of hand and object position as well as interaction forces. In practice, however, control eventually becomes largely data-driven due to its dimensionality and the uncertainty associated with the combined use of its components [6].
Still, data-driven approaches do not come for free. They either require large training data sets [67, 94, 11], restrict the tasks to sufficiently similar scenarios [6, 85], or rely on low-dimensional representations such as synergies [69] and motion primitives [46], that encode the considered manipulation task. Consequently, learned polices inherently couple the employed degrees of freedom, resulting in solutions that are task- and platform-specific. Furthermore, incorporating tactile feedback from all fingers into a control policy quickly becomes intractable given the dimensionality of the feedback signals. In short, low-level control policies that both deal with uncertainty (e.g., in contact locations and forces) and generalize well beyond a limited set of cases, need to be both data-driven and modular.
Ensuring grip stability is central to both stabilizing an object in the hand and moving an object between stable grip configurations. Classical robotics approaches often rely on measures such as form- or force-closure for assessing grip stability but with imperfect models and contact/force sensing, using such measures is very challenging. As a result, many researchers have proposed alternative grasp stability measures [3, 22, 56, 53, 74] and developed accompanying control strategies.
In contrast, human grasping and manipulation appears to be largely data-driven [41] despite relying on feedback signals of huge dimensionality and relatively low precision when control compared to robots. As deduced from several behavioral studies[25, 10, 28], human grasp control strategies seem to be modular and based on local sensing and actuation, rendering the control of the fingers largely independent from each other, i.e., Independent Finger Control [25]. Specific grasps and force distributions appear to emerge from tactile feedback as the fingers interact with objects. Clearly, such an approach would be desirable for robotic grasping and manipulation.

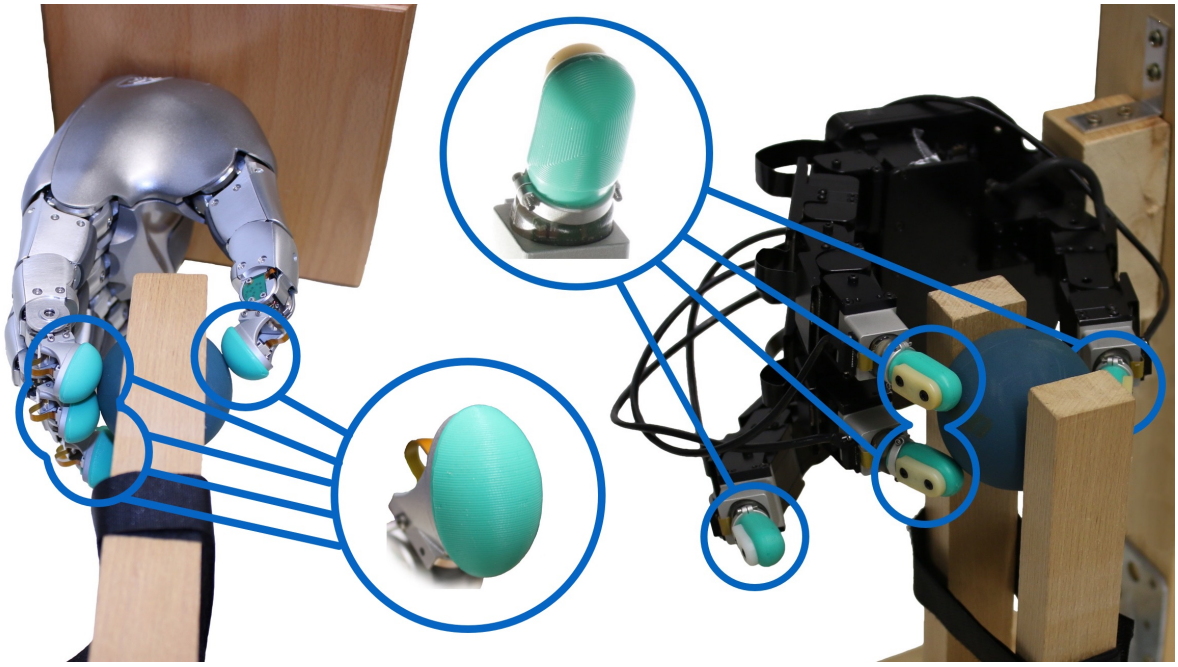

Figure 3.1.: The proposed independent finger grip stabilization controller was successfully evaluated on the Allegro Hand and on the Wessling Hand. The fingertips of both hands are equipped with Syntouch's BioTac or Biotac SP sensors, respectively.

Inspired by progression from one-finger over two-fingers to the whole hand proposed by [70] in the context of tactile object exploration and by the independent control hypothesis in human grip control by [25, 10], we have developed independent control policies based on tactile feedback for each finger that in conjunction generalize from one-finger to five-finger gripping and in-hand manipulation.

To achieve this, we equipped the robotic fingertips of two hands with multimodal fingertip sensors (BioTac and BioTac SP for the Allegro and Wessling Hand, respectively; Figure 3.1), each with a learned predictive model of future slips based on the tactile feedback acquired during finger-object interactions. The local control laws in each finger counteract future slips, ideally preventing them. The resulting control law is capable of stabilizing objects against other objects (such as a table or a wall), jointly stabilizing objects with more robotic fingers (as in in-hand object stabilization or gripping) or against the hand of a human operator (human-robot joint stabilization). It can also be employed for in-hand manipulation by stabilizing an object with several fingers while one or more fingers move the object within the stable grip. The coordination between modular finger controller occurs only indirectly through the tactile signals observed by each finger.

This modular approach enables a higher-level planning system to operate with less object knowledge while requiring simpler models for control than analytical approaches. In contrast to monolithic data-driven approaches, the proposed reactive control framework therefore can be expected to generalize across multiple tasks, a variety of objects and different robotic platforms. Our approach reproduces findings in human motor control where the absolute amount of force applied by single digits

will always settle just above the minimal amount of forces to prevent slip [41, 25] in static setting.

3.2 Modular Tactile Sensing-based In-Hand Object Stabilization

In this section we first introduce a single finger tactile control approach which works well for stabilizing objects pinned against other objects. We then discuss how this approach can be used in multi-finger settings, i.e., fingers of one robot or those of several agents; see Fig. 2.1 for an experiment where this method stabilized an object jointly with a human finger.

3.2.1 Single-Finger Stabilization based on Slip Prediction

Human ability to preceptually discriminate forces applied by their fingertips is limited (Weber fractions typically 5-10%, [64]). Accordingly, tactile information other than those directly related to fingertip force or pressure seem to be employed in human force adjustment strategies during object grasping. As slipping is directly connected to the stability of the interaction with the environment, it is considered crucial for human manipulation [41]. Thus, for single finger tactile stabilization of objects, we recognize two necessary components [25]: (1) a slip predictor and (2) a force adjustment method based on slip prediction.

3.2.2 Slip Prediction

is formulated as a classification problem [87], relying on a classifier $f(\cdot)$ that predicts the slip state at time $t+\tau_f$, with τ_f representing the prediction horizon (here $\tau_f = 10$, with 10 time steps corresponding to 100 ms). To this end, features $\phi(\cdot)$ of the raw sensor signals $\mathbf{x}_t$ (here a vector $[\mathbf{x}_t, \Delta x]$ where $\Delta x = \mathbf{x}_t - \mathbf{x}_{t-1}$) were extracted for a time window $T = (t-\tau_H) : t$, where τ_H is the tactile history (here $\tau_H = 1$). The slip predictor, i.e., $f(\phi(x_t)$, was trained to correctly label the slip state, c, at time $t+\tau_f$

$$c_{t+\tau_f} = f(\phi(\mathbf{x}_{(t-\tau_H):t})) \tag{3.1}$$

as one of the classes in the set $c_{t+\tau_f} \in \{\texttt{slip}, \texttt{contact}, \neg\texttt{contact}\}$. For an in-depth study of how the feature function affects the detection and prediction of slip, the reader is referred to our previous work [87].

3.2.3 Force adjustment

We defined a control law that converted the predicted slip state, c, at time $t+\tau_f$ into adjustments in the applied normal force. Most robotic hands are controlled in joint or end-effector positions rather than applied forces. To make the controller applicable across a range of robotic hands, our controller therefore adjusted the desired task space velocities, $\dot{\mathbf{s}}_t$, rather than controlling force explicitly. Hence, whenever `slip`

was predicted, we increased the normal force, F_N, alternatively slowly decreasing the force while keeping the object stable, in line what has empirically been found during human grasping. This behavior was achieved by using a leaky integrator

$$y_t = \alpha y_{t-1} + (1-\alpha)L \tag{3.2}$$

to control the task space velocity in the contact normal direction, i.e.,

$$\mathbf{s}_t = \mathbf{N}_t y_t. \tag{3.3}$$

where α is the leakage at each time step and L is the integrator input signal

$$L = \begin{cases} 1 & \text{if } c_{t+\tau_f} = \texttt{slip}, \\ 0 & otherwise \end{cases} \tag{3.4}$$

This integrator thus operated as a smoothing filter which was important given the discrete nature of the slip predictor outputs. In multi-fingered scenarios, any oscillations in the controller response would propagate to other fingers engaged in the grasp and cause instability. The minimum integrator response, y_{min}, necessary to keep the fingertip in stable contact with an object was determined from the first slip after initial stabilization

$$y_{min} = y_t \text{ if } \Delta c = \texttt{contact} \rightarrow \texttt{slip}. \tag{3.5}$$

This implicitly defined the minimum fingertip normal force necessary to prevent slips and made the controller responsive to the prevailing friction at its digit-object interface.

3.2.4 Multi-Finger Gripping by Single-Finger Slip Control

When progressing towards in-hand stabilization and in-hand manipulation, more fingers are required and the complexity of the tasks quickly scales accordingly with hand dexterity. Generally, a higher dimensionality can be coped with either by identifying a lower-dimensional manifold for the problem or by decomposing the problem. Following the core insight in [25] that human multi-finger grip stabilization appears to be accomplished by separate neural circuits that interact through the object instead of via the central nervous system, we hypothesize that *multi-finger robot gripping can be accomplished using the same single-finger stabilization controller on each finger independently*. As a first scenario, we reproduce the scenario in [25], where two humans jointly hold an object using one finger each with the same apparent ease as if a single person use the index finger and thumb of one hand or one finger from both hands. The underlying neural control appeared to be unaffected by the precise task condition. We reproduce this in a human-robot joint stabilization task as shown in Fig. 2.1: the single finger controllers of both the human and the robot worked well together without any precautions.

To fully utilize the dexterous capabilities of the hand, we propose that each hand should be considered a set of independently controlled fingers pertaining specifically to stabilization. This does not, of course, imply independent planning, nor independent making and breaking contact.
A set of independent fingers – in contrast to a fully connected manipulator – allows decomposing the object stabilization control problem such that each finger separately predicts future slip based on tactile sensing, avoiding it by independently adjusting the applied forces. While synchronization only through the tactile feedback may appear counter-intuitive, it actually greatly reduces the dimensionality of the control problem while ensuring that the fingers affect each other only when this is required for object stabilization. As a result, it not only becomes more straightforward to design stabilizing control laws but the synchronization becomes robust.

3.3 Experimental Evaluation

In this section we describe and show the results of the experiments performed to challenge the independent finger control hypothesis, as presented in Sec.3.2.4, when using the control strategy proposed in Sec.3.2.3. We begin by stabilizing several objects with a varying number of fingers, using the Allegro hand, without any external perturbations, Sec. 3.4, and demonstrate that a control strategy working under the proposed hypothesis is able to re-stabilize objects in-hand throughout sequences of externally applied perturbations, Sec. 3.4.1. The presentation of the results is preceded by a detailed description of the robotic platform, of the tactile sensors mounted on the platforms and the sensors used to measure the external perturbations, Sec.3.3.1, and a detailed outline of the procedure used to acquire the ground truth data for the slip classifiers, Sec. 3.3.3.

3.3.1 Experimental Setup: Testing Platform & Tactile Sensors

To demonstrate the independent finger control, the control scheme was implemented on two robotic hands: The Allegro Hand and the Wessling Robotic Hand.
The Allegro Hand (Wonik Robotics GmbH, `www.simlab.co.kr`; Fig. 3.1), is a lightweight four fingered hand with four joints per finger, for a total of 16 actuated degrees of freedom. The thumb has an abduction joint, two metacarpal joints (rotation and flexing) and a proximal joint. The remaining fingers do not have abduction joints and instead have a distal joint. A PD controller was used to control the robot joint positions. One end-effector was defined for each fingertip and their positions were controlled by estimating the desired joint velocities, by means of the Jacobian Pseudo-Inverse, and integrating the estimations to acquire the desired joint positions.
The Wessling Robotic Hand has five modular fingers, each with four joints and three active degrees of freedom (Wessling Robotics, `www.wessling-robotics.de`; Fig. 3.1). A PD controller is used for joint position control and a Pseudo-Inverse Jacobian controller is used for controlling the end-effector position of each finger. The control signals are sent to a real-time machine where the conversion to torque is performed

Figure 3.2.: *Test objects.* The majority of the objects were from the YCB object set [12]; only the tea box and the white plastic cup are not in the original set. The *training set* (white arrows) included 4 objects only: a tuna can, a plastic cup, a ball, and a tea box.

by the Wessling software. section While the Allegro Hand has less fingers, it is more compliant and its workspace is larger than that of the Wessling Hand. The base control loops of each hand operate at different frequencies, i.e., 300 Hz and 1 kHz for the Allegro and Wessling Hand, respectively. However, despite these differences, the slip prediction based controllers were the same, each controller trained on data from the respective fingertip sensors.

BioTac and the BioTac SP tactile sensors (SynTouch Inc., `www.syntouchinc.com`; Fig. 3.1) were mounted the Allegro and Wessling Hand, respectively, and served as fingertips. Both provide multi-modal responses composed of low and high frequency pressure (P_{dc} and P_{ac}), local skin deformations (E), temperature and thermal flow (T_{dc} and T_{ac}). The sensor consists of a conductive fluid captured between a pliable skin and a rigid core. The core surface is covered with impedance sensing electrodes (19 for BioTac; 24 for BioTac SP). The pressure signals are acquired by a pressure transducer, skin deformation is measured through local impedance changes measured by the electrodes and temperature is regulated by a thermistor. All data channels of the sensor are sampled at a rate of 100 Hz. The high frequency pressure signal is acquired internally by the sensor at a rate of 2.2 kHz, but is available for readout at 100 Hz, producing batches of 22 values every 10 ms. Considering all channels and the Pac batch data, the sensors output a total of 44 or 49 values every 10 ms.

Finally, the Optoforce OMD-D20 3D (Optoforce Ltd., `www.optoforce.com`) is an optical force sensor (insets of Fig. 3.6) that was used to measure the magnitude of external perturbations applied on the objects during in-hand re-stabilization experiments. The Optoforce reconstructs the magnitude and direction of the applied force from the values of four light sensitive photo-diodes that detect the amount of reflected light by interior surface diodes. The sensor has a nominal sample rate of 100 Hz.

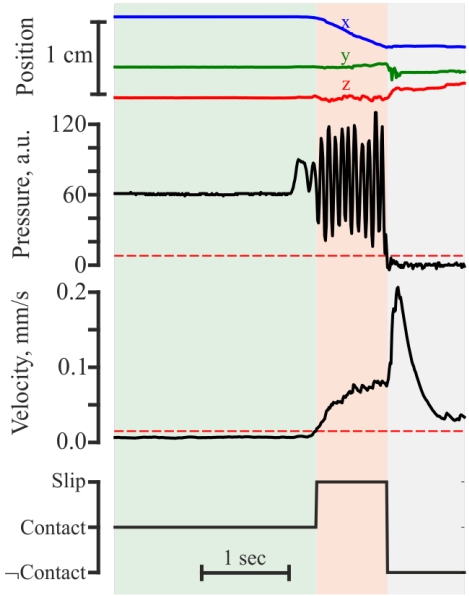

Figure 3.3.: Data from the index finger during a single, representative training trial. The cartesian instantaneous velocity was calculated from differences in finger end-effector position between two consecutive time steps. A pressure threshold, T_{Contact}, and a movement threshold, T_{Movement}, both indicated with red dashed lines, were used to generate the slip ground truth labels shown in the bottom panel.

3.3.2 Test and Training Objects

Our set of 38 test objects belonged with two exceptions (a tea box and a plastic cup) to the YCB object set (Fig. 3.2; [12]). Among the test objects, the weight varied from 10g to more than 400g and grasp width from less than 10 mm to more than 100 mm. Specifically, the plastic cup (cf., Fig. 2.1) was included to assess the performance of the control system when faced with highly deformable objects. Objects were selected to cover a wide range of shapes, sizes and surface properties, as no additional object information (point clouds or models) was used.
Only 4 objects were used during training: a tuna can, a plastic cup, a ball, and a tea box (arrows in Fig. 3.2). Successful manipulation of *all* test objects thus implied that the method generalized across grasps and object properties.

3.3.3 Tactile Training

As our independent finger stabilizers reacted to slip-based feedback, it was necessary to train the classifiers responsible for slip prediction. This training required data collected on the real system and ground truth labels for the slip events.
To start data collection, one of the training objects was fixated by a support in the hands work space (Fig. 3.1). All fingers were positioned in an initial configuration and subsequently flexed until they made contact with the object. Then the pressure

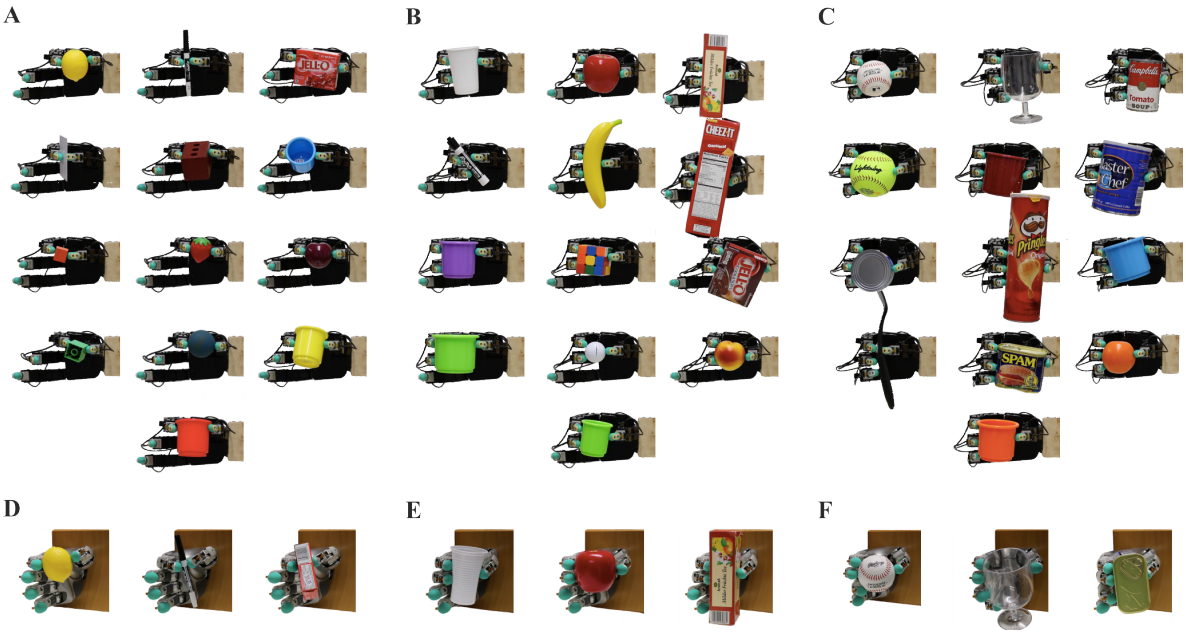

Figure 3.4.: Stable grasps of a variety of objects. The specific grasp configurations varied from trial-to-trial but always resulted in stable grasps. The panels show (A) two-finger, (B) three-finger and (C) four-finger grasps with the Allegro Hand and (D) two-finger, (E) three-finger and (F) four-finger and five-finger grasps with the Wessling Robotic Hand.

applied by each finger was adjusted by a PID controller until a target pressure was reached on each finger. Finally, the fingers moved along the tangential contact plane, surveying the object surface. Acquiring data from three sensors simultaneously reduced the necessary number of training trials. All data from each of the fingers was concatenated into a single data set that was used to train each of the individual slip predictors. The data collection setup is exemplified in Fig. 3.1.

Fig. 3.3 shows a representative, single training trial with data from the index finger. Slip labels were generated automatically from the fingers end-effector location and the recorded pressure values. The total shift in Cartesian position was calculated from the end-effector position. Since the object was fixated during training, we defined slipping as the state when the finger was in contact (i.e., the recorded pressure was above a certain threshold T_{Contact}) and the finger was moving (i.e., the finger velocity exceeded the movement threshold T_{Movement}; both thresholds are indicated with dashed lines in Fig. 3.3).

This procedure relied on randomly selected velocities in task space for the object surface surveying. Target pressures were selected from 9 possible values in sensor grounded pressure units: $P* = [20, 40, 60, 80, 100, 150, 200, 250, 300]$. Spanning the data across multiple pressures in conjunction with randomly selecting the velocity and having distinct contact locations across the three fingers, allowed for training slip classifiers that were not specifically correlated with certain pressures, contact locations or fingertip velocities. In addition, all sensor values concerning pressure or finger deformation were grounded before training, preventing parametric differences in the sensors (for example nominal fluid pressure) from correlating to slip. Three

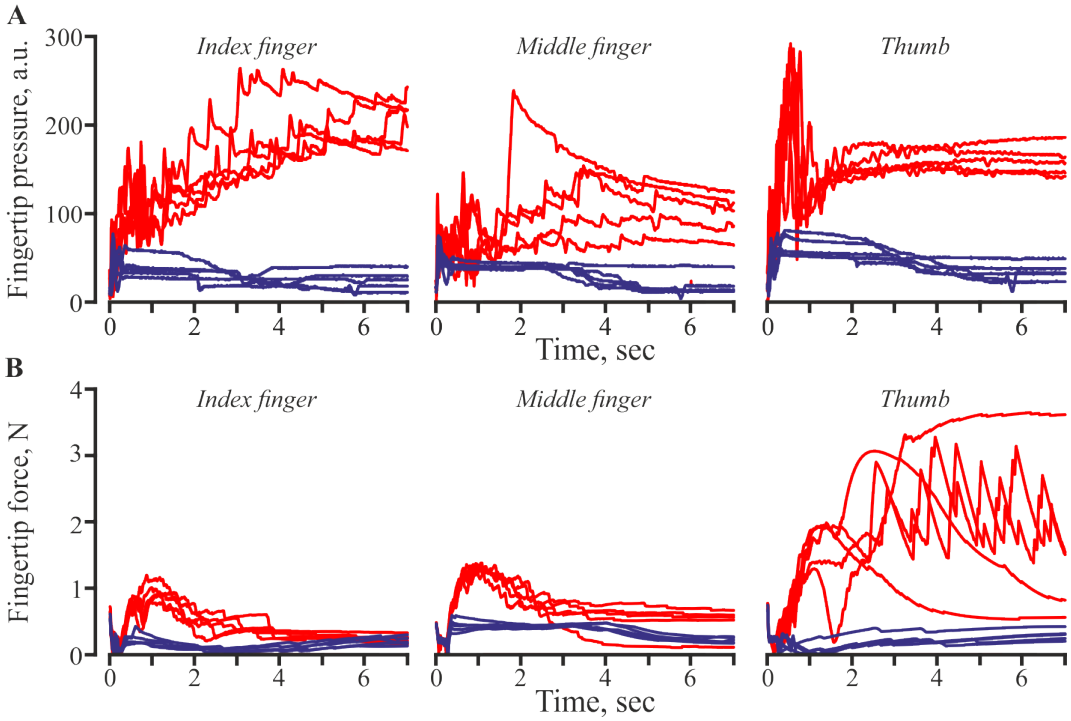

Figure 3.5.: Pressure and force profiles. A comparatively light object (plastic mug; blue lines) or a heavy object (cracker box; red lines) was grasped five times with the Allegro Hand (A) and the Wessling Robotic Hand (B). While all attempts resulted in stable grasps, the exact configuration varied with the fingertip pressures and forces changing accordingly.

trials were executed for each value of $P*$ on four training objects (Fig. 3.2) for a total of 108 trials. The resulting data set is thus comprised of 324 single finger trials across the three engaged fingers and was acquired in less than 15 minutes.

3.3.4 Grip Stabilization Evaluation

For the multi-finger grip stabilization scenarios, finger pressure was analyzed and used to make behavioural comparisons across objects (reported in Sec. 3.4). In addition, we assessed the in-hand re-stabilization capability of our approach as the grip was perturbed by an external agent (Sec. 3.4.1).
Since each finger was controlled independently, the approach was scalable with respect to the number of fingers. In this study, however, we considered grip configurations involving two and three fingers across all test objects (Fig. 3.2) including the four objects used in the slip predictor training data collection experiments.

3.4 Multi-Finger Grip Stabilization with Independent Finger Control

To test the validity or our independent finger control hypotheses for grip stabilization, we attempted to stabilize multiple objects with varying number of finger.
We place the robotic hand in an open-hand configuration with an object positioned such that it could be held in an opposition grasp, and then closed two or more fin-

gers (up to four with the Allegro Hand and up to five with the Wessling Robotic Hand). Immediately after all fingers have contacted the initially supported object, the grip stabilizers were activated and the independent finger stabilization process began, while the object support was removed. To ensure that the object was not dropped as soon as the stabilizers were activated, each controller was initialized to generate a half of the maximum output ($y_0 = 0.5$). For deformable objects such as the white plastic cup, this resulted in an initial surface deformation that was subsequently automatically reduced.
The control based on independent finger control was able to reliably and consistently stabilize all 39 test objects (Fig. 3.4). For each object and grasp configuration (two-, three-, four-finger grasps with the Allegro Hand and up to five-finger grasps with the Wessling Hand), we recorded five trials each lasting 10 seconds with every object. A grasp was considered stable if the object was not dropped.
Since no desired hand configuration was enforced, the hand adopted slightly different configurations for each object and across repetitions. To study this variability in more detail, we analyzed the grip forces applied by the fingers to different objects.
Figure 3.5 depicts the changes in force distribution for the duration of trials with the lightest and the heaviest objects, i.e., the white plastic cup and the cracker box.
Since no direct force readings are available from the Allegro hand, pressure values measured directly from the BioTac sensors are used instead. For the experiments with the Wessling hand, forces applied were estimated from joint torques and angles. The data illustrates two important emergent properties of the grasp control. First, finger pressures and forces converged to lower values when gripping the lighter plastic cup than when gripping the cracker box. Second, there was a substantial variability in force sharing between the digits across trials, particularly obvious in the profiles recorded during trials with the cracker box. Both of these observations can easily be explained given the design of the controller. Notably, an uncountable number of grip force distributions could result in stable grasps but the control system did not explicitly enforce a specific distribution. Instead, pressure applied by each finger propagated through the object to the other fingers, dynamically impacting the grip force distribution while each controller minimized the risk for local slips keeping the fingertip forces low. The ability to adapt the overall grip force by reactively changing the force applied by each finger contributed to the high generalization capability of our approach, even though no specific object orientation, weight or weight distribution was expected by the stabilizers.

3.4.1 Grip Stabilization under External Perturbations

To further test the validity of our control hypothesis, we investigated responses to externally applied perturbations (Fig. 3.6). Once the object was stabilized in the robotic hand, the experimenter held an Optoforce and used it to disrupt the object state by applying sequences of irregular disturbances, either to the different surfaces of the objects or to the fingertips, during 30 second recording periods (insets in Fig. 3.6).
For the entire duration of these experiments, the stabilizers invariably counteracted the perturbations successfully by adapting the finger pressures. With every perturbation, we observed a change in the fingertip forces and an increase in the accumulated

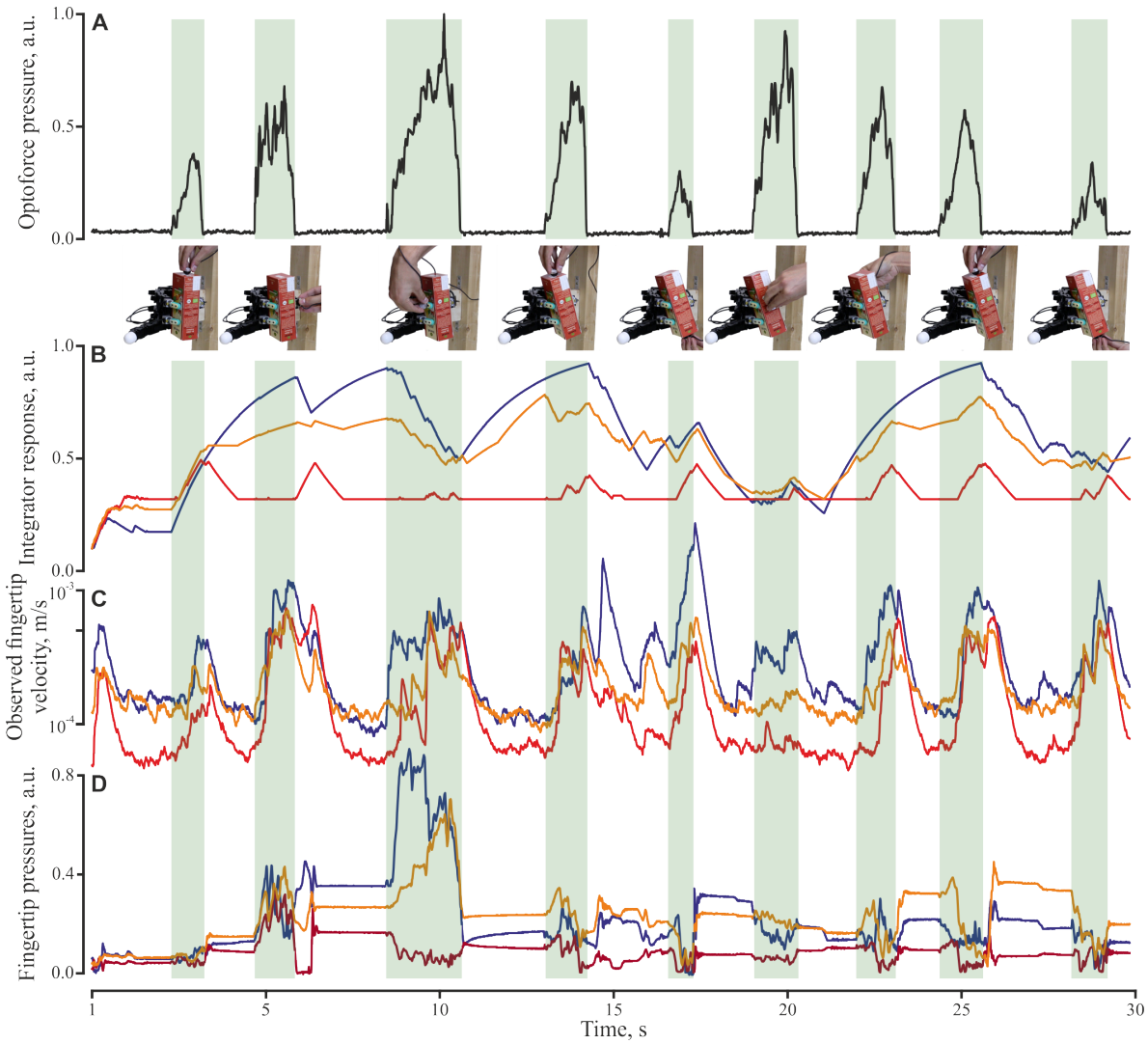

Figure 3.6.: Responses to external perturbations. The panels show (A) the pressure applied by the experimenter on the surface in the manner shown in the insets, (B) the integrator response of the controller that drives the fingertip velocities (C) the observed fingertip velocities and (D) the applied fingertip pressures by the thumb, index and middle fingers (yellow, blue and red lines). As each controller continuously predicted the contact state 100 ms in the future, the output of their leaking integrators increased whenever a slip was predicted, otherwise allowing the integrator output to decrease slowly to a minimum value. The integrator response determined the necessary fingertip velocity, thereby implicitly managing the applied pressure against the object surface.

value of the integrator that regulated the applied velocity. As a result, the individual fingers applied slightly different forces after each perturbation. For instance, the 1st, 4th and 8th perturbation in Figure 3.6 were applied in a similar fashion (i.e., from top) but in response, the independent finger controllers generated different stable grip force distributions. Indeed, while the object was held in a similar position throughout this trial, the pressure distributions across the fingers differed follow-

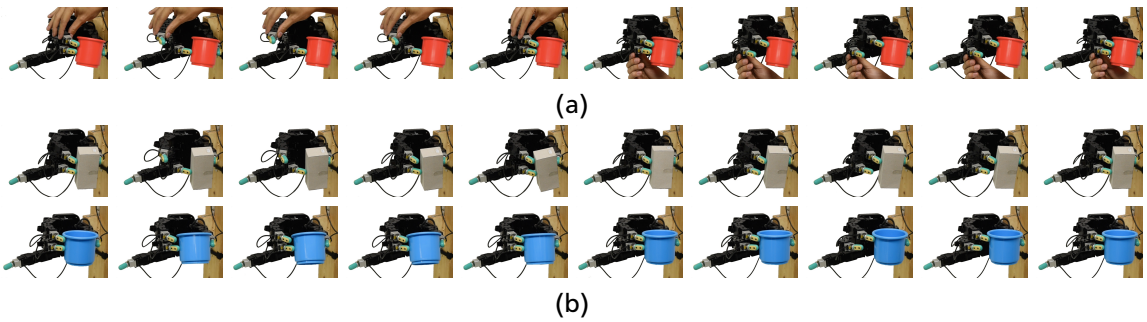

Figure 3.7.: In order to remove the human from the master-slave experiment, (a) an experimenter provides demonstrations used to learn Probabilistic Movement Primitives (PROMP) that (b) when reproduced on a box and a cup move the index finger away and towards the object, creating a finger gaiting motion. During PROMP execution, the remaining fingers rely on the independent finger stabilizers to keep the object stable.

ing each perturbation. Changes in fingertip forces due to slip prediction noise or re-stabilization were also frequently observed (e.g., around 16 and 21 second mark). From the perspective of the independent fingertip controllers, there was no or little difference between external perturbations and those caused by the actions of other fingertips. This was further explored in master-slave experiments during which the experimenter manually pushed or pulled a finger to increase or decrease the force it applied while the controllers of the remaining fingers jointly stabilized the grasp. Indeed, three- and two-digit grasps remained stable even when one of the digits was lifted off the surface of a grasped object. For the particular case of pulling the thumb, the number of fingers in the grasp remains the same, with the index and middle fingers compensating for the thumb movements. In contrast to more traditional solutions for manipulation control, force sharing between the engaged fingers varied substantially from trial-to-trial due to the emerging nature of the independent finger control policy. Such variability is, however, typical in human manipulation [25, 10, 28, 9], and therefore does not per se imply poor control. In grasping and in-hand manipulation, instability is synonymous with slip [84]. In this study we have focused on low-level control of grasp stability rather than finger positioning and re-positioning. However, we wished to evaluate if the behaviors observed in the master-slave experiment could be automated, eliminating the human from the loop. To achieve this automated master, we had an experimenter provide perturbation demonstrations where contact between the object and the index and middle fingers is broken by pulling each of the respective fingers. These demonstrations are then used to train Probabilistic Movement Primitives (PROMP) [65], which are then executed alongside the independent stabilization controllers. As in the previous master-slave experiment, the independent stabilizers keep the object firmly gripped while the PROMP pulls and pushes one of the fingers away from the object. Snippets of both the demonstration and of the behavior observed when executing the PROMPS are depicted in Figure 3.7. All the results show so far suggest that independent fingertip control at the base level of a hierarchical control framework may enable higher level control policies to perform complex manipulations. In a basic scenario, rotating an object, for instance,

would simply require that one of the fingers introduce a desired perturbation to the object, while the remaining fingers keep it stable.

3.5 Conclusion and Discussion

In this section we summarize our analysis of the proposed independent finger control approach. The controllers are capable of stabilizing grips involving multiple objects of different shapes, sizes and weights purely be reacting to individual slips at the fingertips suggesting that such controllers could serve has the low level controllers of a hierarchical control approached for in-hand manipulation.

3.5.1 Summary of the Contribution

We have corroborated the hypothesis that stable grasps emerge from a set of independent finger controllers. Indeed, the synchronization between fingers emerge from the tactile feedback of each finger controller and enable stable gripping despite disturbances caused by poor contact distribution on the fingertip surfaces, introduced by other fingers action on the object, or external disturbances. Each finger thus automatically compensated for changes that jeopardized grasp stability. Moreover, our modular control approach was shown to be generalizable across multiple objects, even objects that were substantially different from the objects in the training set.

3.5.2 Recognized Shortcomings

Using the low dimensional slip signals defined in previous work [87], enabled the design of the controller used in this chapter. As the full tactile state is much richer than the slip signals, we may have discarded relevant information.
Additionally, in this work, we focused on 'low-level' control of grasp stability. As such, the objects tested were provided to the hand in configurations where the stabilization would be possible, requiring neither finger gaiting nor re-positioning. The initial grass direction also remained constant, avoiding shifts in the direction of gravity.
The implemented controller is reactive, albeit that upcoming slips are *predicted* by the controller, as shown in the previous chapter. The temporal limitations in this respect have not been analyzed. For comparison, it takes human as much as 60-80 ms to initiate force responses to incipient and overt fingertip slips and at least 50-100 ms to generate substantial counteracting forces [44, 32], i.e., these delays are too long for preventing the loss of a stable grasp once overt slippage occurs.

3.5.3 Future Work

Partitioning the hand into a set of independent fingers allows the manipulation problem to be viewed as a distributed problem where each finger solves the task locally. This invites simpler control models than when considering a complete model for the full hand. Specifically, we consider it realistic to use data driven approaches that take

into account a richer sensor space, as the dimensionality of the problem is distributed across the fingers. Our future work will focus on exploring the high dimensionality of the feedback signals and learning stabilization controllers using reinforcement learning approaches in these high dimensional spaces.

Our results invites exploration of master-slave paradigms. In a simple scenario, rotating an object would simply require that one of the fingers introduce a desired perturbation to the object, while the remaining fingers keep it stable.

Finally, for complex manipulations, we posit that independently controlling the fingers will be necessary but not sufficient to achieve robust performance. Using the independent control as the base level in a hierarchical control framework is expected to enable higher level control policies to perform these manipulations, effectively creating a robust control hierarchy, where the task complexity is distributed across the several levels of the hierarchy. Building such a hierarchy is thus a potentially interesting future work.

4 Hierarchical Control Decomposition of Dexterous In-Hand Manipulation Tasks

4.1 Introduction

Dexterous in-hand manipulation is a long studied problem, involving precise movement, inter-finger coordination, and contact management [62]. While manipulating objects within a grip is possible with simple grippers, external forces such as gravity or interactions with the environment are necessary to generate movement [14, 80, 20]. When considering dexterous hands, the problem complexity greatly increases [54], as the additional fingers allow for an increased number of possible solutions for each manipulation action and a larger number of possible interactions with objects. Traditional in-hand manipulation control approaches tackle simplifications of the general problem by attempting small movements or by relying on several strong assumptions regarding contact and the precision of the available robot and object models [2, 98, 57]. Even with such simplifications, experiments on real robot platforms are prohibitively hard and thus frequently omitted in the literature [2, 98]. Seeing in-hand manipulation as a planning or optimization problem provides solutions for more general forms of the problem, but most of these solutions integrate very little to no feedback [82, 61, 15, 75]. Considering feedback during task execution is crucial to tackle the variability introduced by objects, in the form of distinct shapes, surface properties, target movements or initial grasp configurations. To achieve a sufficiently general solution to in-hand manipulation, manipulation controllers not only have to generate suitable trajectories that take into account task variability, but also have to adapt in accordance with the feedback signals observed during task execution to compensate for unforeseen events, such as object slip.

Tactile sensing is an attractive form of feedback for in-hand manipulation, as it provides information directly from the interaction points. It also offers substantial advantages over other forms of feedback such as vision and force, by disregarding effects such as occlusion while providing rich information at high frequencies [96]. It has also been shown to help with interaction variability required for in-hand manipulation, as it enabled objects to be grasped robustly regardless of their shape or material properties [86]. However, integrating high dimensional tactile feedback signals in the control loop of an already complex in-hand manipulation controller is non-trivial.

Reinforcement Learning (RL) has found great success in solving control tasks with large input spaces on both simulated [60, 78] and physical platforms [51]. Thus, several approaches based on reinforcement learning [68, 85, 85, 63], learning from demonstration (LfD) [53], combinations of RL and Lfd [71, 31], or optimal control

with learned local models [48] have been proposed for in-hand manipulation. Despite this, when considering complex tactile sensors such as the BioTac [91], the richness of the feedback signals leads to considerably more complex state spaces and transition functions, yielding significantly more challenging RL problems. For example, pressure on different contact points of the BioTac sensors is measured from the displacement of fluid within the fingertip which results from the deformation of its malleable skin. Such a complex physical process is currently impossible to simulate accurately and efficiently. Hence any RL policy learned in simulation using a model of the tactile sensor would likely not transfer to a physical robot. On the other hand, learning the task directly on the robot is hardly feasible because i) in-hand manipulation tasks are contact-rich, which creates non-linearities in the state transitions and precludes the learning of a forward dynamics model in a model-based RL setting and ii) the high dimensionality of the tactile sensors precludes the use of model-free RL directly on the robot due to a prohibitively high sample complexity. Accordingly, only [85] use RL with integrated tactile information by training the policy directly on a real robot and using very simple tactile information. Additionally, the task is constrained during training by having the object supported by an external surface that prevents it from falling.

Constraining the manipulation task to instances where the object is in a supported position (either by the palm of the robot or by an external support surface), such that the object is less likely to be dropped during exploration, is common among several proposed approaches [71, 48, 85, 63]. The use of such a constrain is justified by the unwieldy nature of the transition function of in-hand manipulation tasks, even in simulated environments. Indeed, if the robot is holding an object as in Fig. 4.1, any exploratory action (a random perturbation to the current joint position) is likely to make the object fall and thus terminates the trajectory after only a few number of steps. We observed that such exploratory behavior could lead to premature convergence of RL to poor local optima where the robot reinforces behaviors that throw the object towards the target. This results in a short term accumulation of rewards at the detriment of the longer term rewards. In addition, we observed that methods such as the ones used in [63] to produce impressive results on a real robot with the object supported the palm, are unable to learn the task when the support is removed.

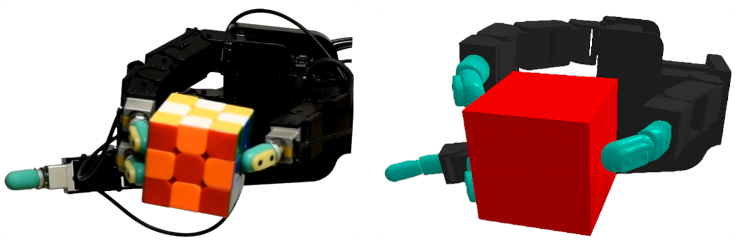

(a) (b)

Figure 4.1.: The real (a) and simulated (b) Allegro hands that were used in our experiments. The tactile information provided by the sensors on the real platform is abstracted in simulation using our proposed hierarchical control decomposition.

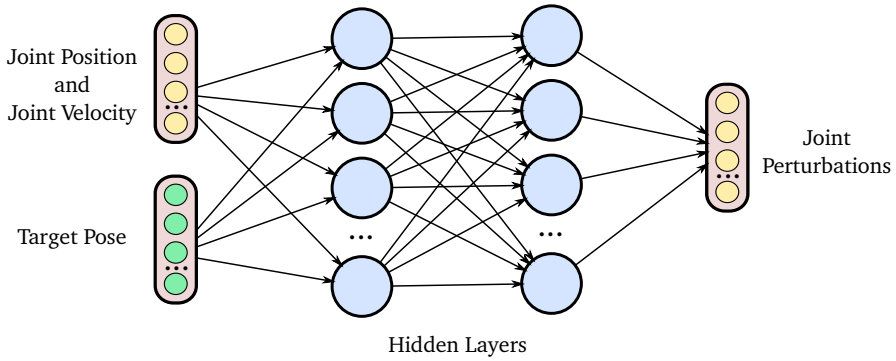

Figure 4.2.: Overview of an non-hierarchical policy network. The network takes joint positions q, joint velocities $\dot{q}$ and the target pose T as inputs, outputing a set of perturbations to the current joint position u_{mov}.

To address both the learning of in-hand manipulation tasks with rich tactile feedback and the relaxing of the support constraint, we propose a hierarchical control decomposition that relies on a low-level composed of a set of stabilization controllers to stabilize the object in-hand during the manipulation actions. These low level stabilization controllers have the benefits of i) enabling the efficient learning of complex in-hand movements in simulation by maintaining the object in the robot's hand for a longer period of time, transforming the transition function to a less unwieldy one and ii) potentially allowing transfer of policies learned in simulation to physical environments by abstracting tactile information and letting the upper level policy be solely defined on joint information. The stabilization controllers are the independent finger stabilization controllers introduced in Chapter 3. We show that with the proposed hierarchical decomposition RL methods are able to learn complex and generalizable manipulation actions, provided that the finger stabilizers keep the objects withing the grip.

4.2 Hierarchical Control Decomposition for In-Hand Manipulation

In order to learn general manipulation policies in simulation, that can potentially transfer to a physical robot, we propose a hierarchical control decomposition composed of two control levels: a set of grip stabilization controllers running independently on each finger and a manipulation movement policy that produces the movement trajectory in joint space and trades-off between manipulation and stabilization. We begin by defining the RL problem in a non-hierarchical fashion, follow with a description of the stabilizers that compose the low-level of our proposed hierarchical decomposition and showcase the differences between the non-hierarchical and the hierarchical learning problems.

4.2.1 Reinforcement Learning Problem Definition

Given an initial grasp on an object, we consider the in-hand manipulation task of translating and/or rotating the object to a target pose. We phrase this problem as

a Markov Decision Process (MDP), defined by the quintuple (S, A, R, P, γ), where S is a state space, A the action space, $P(s_{t+1}|s_t, a_t)$ the transition probability, $R(s_t, a_t)$ its associated reward, and γ is the discount factor. In a non-hierarchical RL setting (NH-RL), the state space is comprised of joint positions q, joint velocities $\dot{q}$ and target pose T. The action space is the set of perturbations to the current joint position u_{mov}, constrained by a maximum tolerated velocity. The structure of the non-hierarchical neural network policies is depicted in Fig. 4.2. The reward $R(s_t, a_t)$ is inversely proportional to the distance between the current and target object coordinates.
Let π be a stochastic policy giving the probability $\pi(a|s)$ of executing action $a \in A$ in state $s \in S$. Let the Q-function be $Q_\pi(s,a) = \mathbb{E}\left[\sum_{t=0}^{\infty} \gamma^t R(s_t, a_t) \mid s_0 = s, a_0 = a\right]$, where the expectation is taken w.r.t. all random variables s_t and a_t for $t > 0$. Let $V_\pi(s) = \mathbb{E}_{a\sim\pi}[Q_\pi(s,a)]$. The goal of RL is to find the policy maximizing the policy return $J(\pi) = V_\pi(s_0)$ where s_0 denotes some initial state (an initial grasp in our case).

4.2.2 Independent Grip Stabilization Control

The stabilization controllers that compose the base control level where introduced in [86], and are deployed on each finger independently. By interpreting the tactile signals provided by the BioTac sensors [91], these independent finger stabilizers (IFS) locally avoid predicted slip events. This allows them to keep objects stable within multi fingered grips while not being constrained to a particular grasp configuration or a particular distribution of force between the fingers. In a hierarchical setting, the main task of the stabilizers is to ensure grip stability throughout the manipulation action. Formally, provided with a label $c_{t+\tau_f} \in [\text{slip}, \neg\text{contact}, \text{contact}]$ from a learned tactile based slip predictor, the levels of a leaky integrator are adjusted as follows

$$y_t = \alpha y_{t-1} + (1-\alpha)L \tag{4.1}$$

where α is the leakage at each time step and

$$L = \begin{cases} 1 & \text{if } c_{t+\tau_f} = \texttt{slip}, \\ 0 & \text{otherwise} \end{cases} \tag{4.2}$$

is the integrator input. The integrator value is then used by the stabilizer to regulate the desired task-space velocity in the contact normal direction, i.e.,

$$\mathbf{v}_{\text{stab}} = \mathbf{N}_t y_t, \tag{4.3}$$

where $\mathbf{N}_t$ is a unit vector pointing in the contact normal direction. In short, the integrator changes with the predicted contact state, accumulating its response when `slip` is predicted and leaking if `contact`. Finally, the stabilization disturbances to the joint positions of the i-th finger $\mathbf{u}^i_{\text{stab}}$ are calculated using inverse kinematics. There are three differences in implementation pertaining to these controllers between the simulated and real robot environments. The first, is the manner in which the normal contact direction is acquired. In simulation, the contact normal is acquired via the

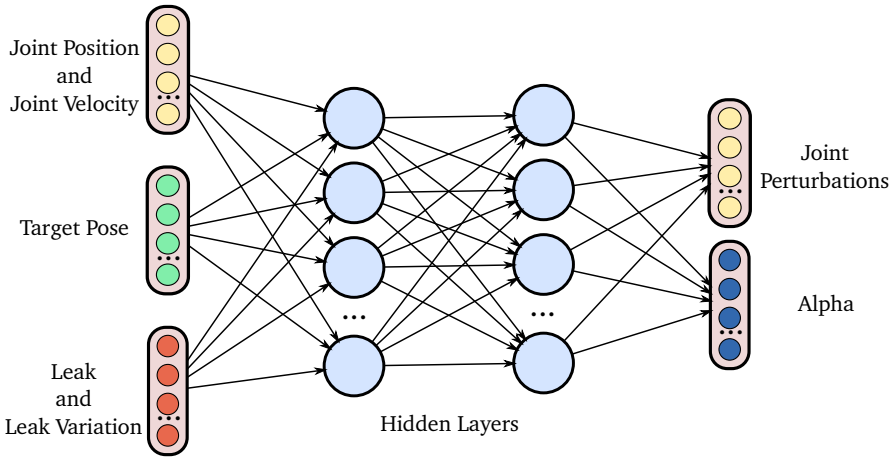

Figure 4.3.: Overview of the high level policy network that produces the manipulation movements. As in the NH-RL case, the network takes joint positions q, joint velocities $\dot{q}$ and the target pose T as inputs but now also receives leakage y and leakage variation Δy information. The movements are once again represented by a set of perturbations to the current joint position u_{mov}. The network now also outputs the merging coefficients α_i between the movement commands $\mathbf{u}_{\text{mov}}$ and each of the stabilizers responses $\mathbf{u}^i_{\text{stab}}$.

simulator's collision engine while the real robot estimates it via the weighted average of the normal directions of the electrodes. The weights are the activations of each electrode as described in [92]. The second difference concerns the intensity of the stabilizer response. Due to fluctuations of the fluid of the real sensors, pressure values might indicate that there is no longer contact for one time step, creating jerky responses. As in [86], the controllers of the real robot do not immediately stop whenever contact is lost, but have their response smoothly reduced over a period of 200 ms. The final difference concerns the slip signals used by the stabilizers. In simulation, slip signals are provided by a perfect slip detector, that observes the changes in relative position and orientation between the fingertip and the object to detect slip. In the real robot, slip is predicted from learned tactile based slip predictors, as described in [86], and a prediction window τ_f of ten is used.
The stabilization controllers are independent of the nature of the manipulation task (e.g. nature of the manipulated object, target coordinates or type of initial grasp) and do not need to be learned. Most importantly, they provide an abstraction to the tactile information provided by the sensors, allowing the high level movement policy to not depend on tactile information while the overall system still reacts to tactile feedback. Being able to learn movement policies with information that is readily available to both the simulated and the real robot potentially facilitates the transfer of policies between the two.

4.2.3 In-hand Manipulation Movement Policy

To generate the manipulation movements, a high-level policy π_θ, parameterized by the weights of a neural network θ, is learned in a simulation environment depicted

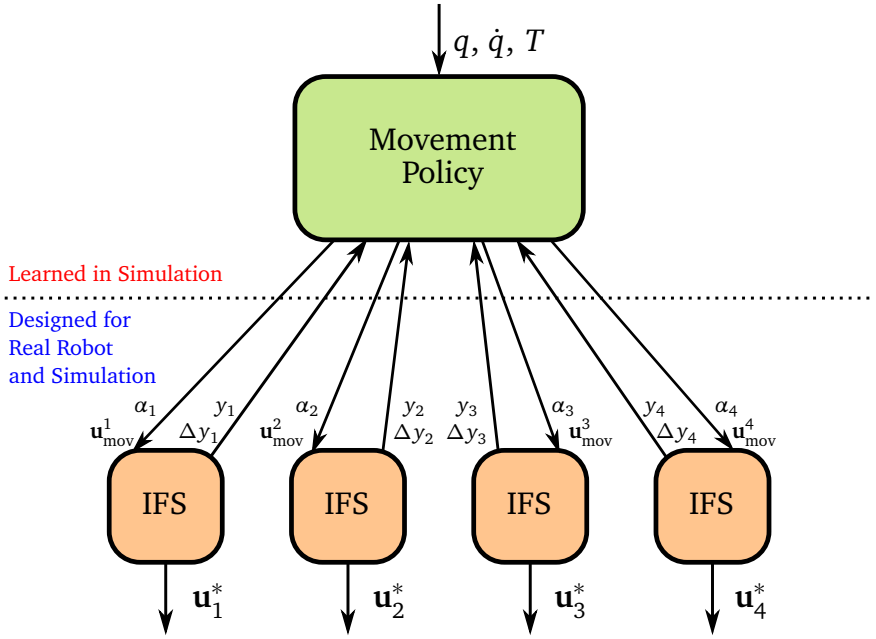

Figure 4.4.: The proposed hierarchical structure. The movement policy has access to joint positions q, joint velocities $\dot{q}$ target pose T, and the internal state variables of each of the individual stabilizers y_i and Δy_i. To each stabilizer, it transmits a set of joint perturbations $\mathbf{u}^i_{\text{mov}}$, that generate the necessary finger movements, in addition to a coefficient α_i used to merge movement and stabilizing perturbations $\mathbf{u}^i_{\text{stab}}$, and generate the final command u^*_i.

in Fig 4.1b. In contrast to the NH-RL case, in the hierarchical RL (H-RL) setting, the new state space S' is not only comprised of joint positions q, joint velocities $\dot{q}$ and target pose T but also includes the leakage $\mathbf{y} = [y^1, ..., y^4]$ and the leakage variations $\Delta\mathbf{y} = [y^1_t - y^1_{t-1}, ..., y^4_t - y^4_{t-1}]$ of all the finger stabilizers. The action space is also different, with the new action space $A' = A \times [0,1]^{N_{\text{fing}}}$, now including a set of N_{fing} uni-dimensional merging coefficients α_i, where N_{fing} is the total number of fingers, in addition to the movement commands in the form of perturbations to the hand's joint positions $\mathbf{u}_{\text{mov}}$, that were already included in the action space A. The merging coefficients α_i regulate the combination of both perturbations, $\mathbf{u}^i_{\text{stab}}$ and $\mathbf{u}_{\text{mov}}$, to compose the final action. Letting $\mathbf{u}_{\text{stab}}$ be the combined response of each individual finger

$$\mathbf{u}^* = \alpha\mathbf{u}_{\text{mov}} + (1-\alpha)\mathbf{u}_{\text{stab}}. \tag{4.4}$$

Fig. 4.3 depicts the high-level movement policy of the H-RL setting while Fig. 4.4 provides an overview of the proposed hierarchy. The latter also re-emphasises the fact that low-level is designed both in simulation an on the real robot, allowing the high-level policy to rely solely on joint space information.

An important set of hyper-parameters in our hierarchical decomposition is the initial distribution of each α_i, in order to obtain maximum variability in the trajectories of the initial policy and facilitate the RL process. Low values of α_i have the desired

effect of stabilizing the grip but dampen the variability of the initial trajectories. Similarly, high values of α_i produce trajectories with low variability as the object falls almost immediately. To find an appropriate trade-off we manually tune the hyper-parameters governing the distribution of α by visual inspection of the resulting initial policy in simulation. The resulting distribution for each α_i is a Gaussian with mean 0.5 and a variance of 0.25. By centering the distribution at the transition point between the stabilization and the movement perturbations, we allow for exploration movements with stabilizer compensation. The variance being relatively low prevents sudden shifts from full movement to full stabilization perturbation and vice-versa.
Any RL algorithm can be applied to this hierarchical decomposition as the actions are not time-extended. Learning proceeds as follow: at the start of an episode a random target coordinate is sampled and the policy is executed until the object falls or ten seconds have elapsed. Upon collection of the trajectories we use TRPO [76] to update the neural network policy depicted in Fig. 4.3. In our experiments, the same implementation of TRPO [23] is used to compare both NH-RL, and the proposed H-RL to in-hand manipulation.

4.3 Experimental Evaluation

Using a simulated environment, we evaluate the efficiency of our proposed H-RL when compared to NH-RL. We also analyze how the learned H-RL policies generalize to other manipulation actions. Finally, we present preliminary results on transferring H-RL policies learned in simulation to a real robot platform.

4.3.1 Experimental Procedure, Testing Platform and Tactile Sensors.

All experiments are performed either on a simulated or real version of the Allegro Hand that is equipped with BioTac fingertip sensors (SynTouch Inc., `www.syntouchinc.com`). The Allegro Hand (Wonik Robotics GmbH, `www.simlab.co.kr`), is a four fingered hand with four joints per finger, for a total of 16 actuated degrees of freedom. With the exception of the thumb, all fingers have two metacarpal joints (rotation and flexing), a proximal joint and a distal joint. The thumb does not have a distal joint having an abduction joint instead. A PD controller was used to control the robot joint positions with a control loop that runs at 300 Hz.
BioTac tactile sensors [91] were used as fingertip sensors. The sensors provide multi-modal responses composed of low and high frequency pressure (P_{dc} and P_{ac}) captured by a pressure transducer, local skin deformations (E) acquired through local impedance changes measured by 19 electrodes scattered across the sensors core surface, as well as temperature and thermal flow (T_{dc} and T_{ac}) measured by a thermometer. All data channels of the sensor are sampled at a rate of 100 Hz. The high frequency pressure is sampled in batches of 22 values at the same frequency. Considering all channels and the P_{ac} batch data, the sensors outputs a total of 44 values every 10 ms.
The PyBullet simulation environment [17] is used to simulate the hand and the fingertip sensors. The PD control gains of the hand were tuned in simulation to emulate

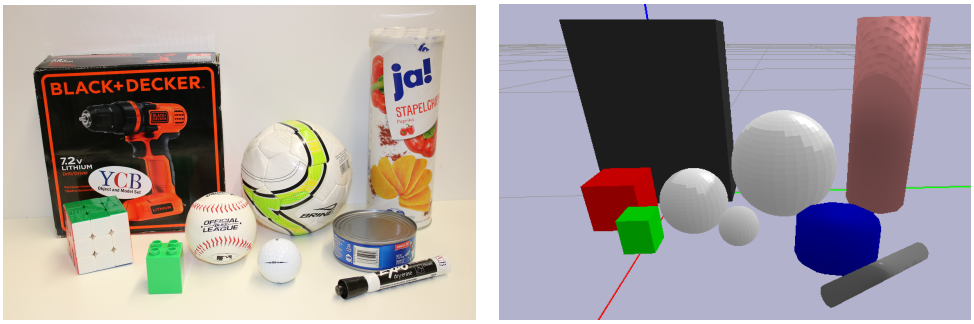

(a) (b)

Figure 4.5.: The real (a) and simulated (b) objects used in our experiments. The objects are a subset of the YCB object and model data set [12]. Since the stabilizers implemented here have a fixed response along the normal direction, the chips can of the data set was replaced by a similar but empty chips can in order to avoid manipulating heavier objects.

the behavior of the real hand. The BioTacs are not simulated. Instead information of contact force and normal direction is obtained directly from the collision engine. In addition to the simulated slip stabilizers, a simplified version of the stabilizers where a constant desired velocity factor β is used for comparison

$$\mathbf{u}^i_{\text{stab}} = \beta \mathbf{N}_i. \tag{4.5}$$

All experiments are performed on a subset of objects from the YCB object and model set [12], either simulated or on the real robot, as shown in Fig. 4.5.

The simulation experiments considered three possible initial configurations: two fingered grasps for the green Lego brick, the golf ball and the marker, three fingered grasps for the Rubik's cube, the baseball and the tuna can and finally four fingered grasps for the screw-driver box, the small football and the chips can. Each of these stating configurations served as the initial pose for four different manipulation movements. These movements were sampled at the beginning of each trial different target positions and target orientations, both with respect to the initial object position. The position targets are sampled from a set of two positions, attempting to move the object by 2cm to the edge of the work space with respect to the y axis. The hand is oriented such that x is the axis moving away from the palm, y the axis pointing from the palms to the fingers when the fingers are in a stretched position, and z is the height. Rotation targets are either positive or negative $\pi/4$ rotations around the initial position with the sign sampled uniformly at random. Having four combinations at the edge of the work space allows all target poses to be consistently observed every episode, simplifying the learning process while potentially allowing the policy to generalize to other intermediate poses. Five learning trials were performed for each combination of manipulation/object configuration and target movements with 50 million samples per trial.

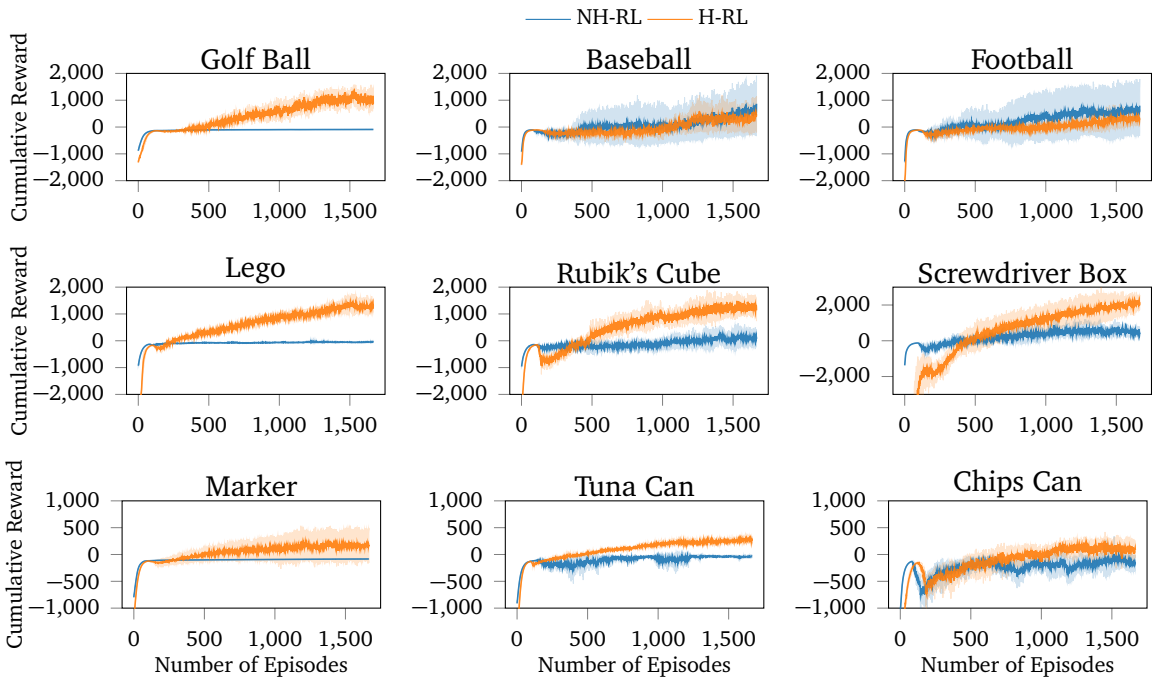

Figure 4.6.: Cumulative reward curves for H-RL and NH-RL, both trained with TRPO. H-RL outperforms NH-RL for smaller objects but the gap in accumulated rewards significantly decreases with object size, with NH-RL showing similar or slightly higher accumulated reward values for larger objects.

Regarding the learning process, the reward function R is given by

$$R(s_t, a_t) = F(P_{err} + O_{err}) - \mathbf{a}_{cost} - \mathbf{a}_{cost} - d \tag{4.6}$$

where P_{err} and O_{err} respectively correspond to the position and orientation terms

$$P_{err} = e^{(\mathbf{p}_{curr} - \mathbf{p}_{des})^2} \tag{4.7}$$

$$O_{err} = e^{(\mathbf{o}_{curr} - \mathbf{o}_{des})^2}. \tag{4.8}$$

In order to produce structured manipulation movements, we enforce that the number of fingers in the initial grasp is maintained throughout the manipulation action. This is achieved via F, a ratio between the number of fingers initially in contact with the object K and the current fingers in contact with the object

$$F = \frac{1}{K} \sum_{k=0}^{K} f_k \tag{4.9}$$

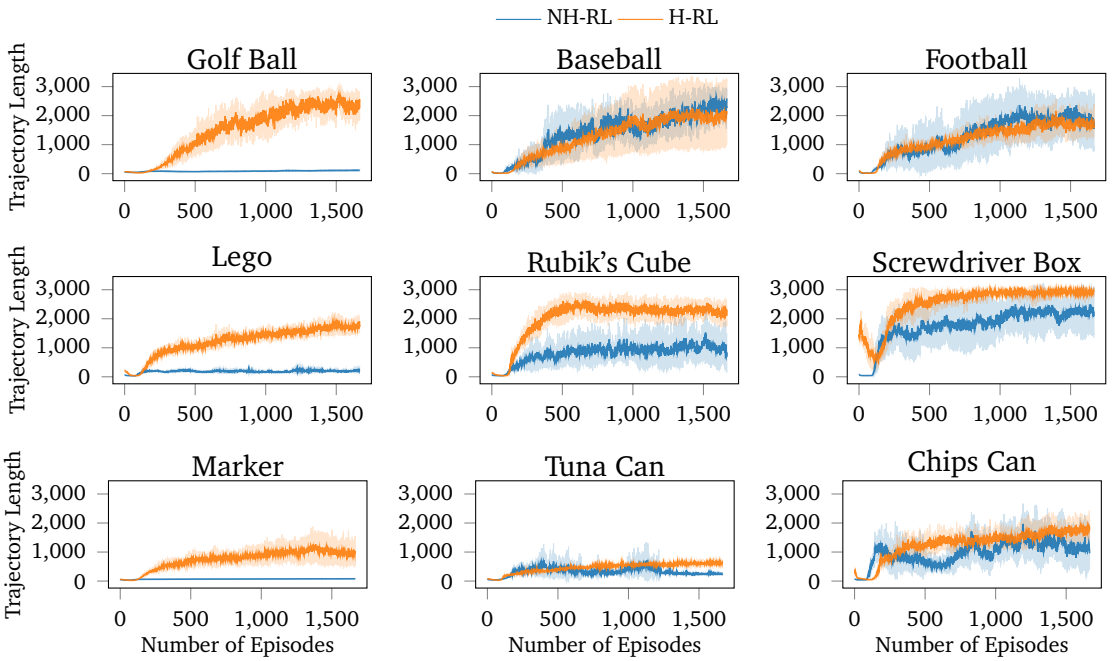

Figure 4.7.: Evolution of the average trajectory lengths achieved by both NH-RL and H-RL with the number of learning episodes. The critical effect of the RL's exploratory actions is evident for smaller objects, where NH-RL is unable to increase the trajectory length, and hence unable to learn.

where f_k equals one if kth finger is in contact and is zero otherwise. We also wish to enforce smooth movement during the manipulation action. We do so by applying costs $\mathbf{a}_{cost}$ and $\mathbf{a}_{cost}$ on the velocity and acceleration respectively

$$\mathbf{a}_{cost} = \sum_{i=0}^{J} (a_t^i)^2 \tag{4.10}$$

$$\mathbf{a}_{cost} = \sum_{i=0}^{J} (a_t^i - a_{t-1}^i)^2 \tag{4.11}$$

where J is the number of joints. Finally, d is a negative penalty given when the object is dropped.

In addition to the previous reward terms, a specific term is added to the reward calculation in the H-RL setting. This term is an additional cost

$$\alpha_{cost} = \sum_{i=0}^{N_{\text{fing}}} (\alpha_t^i - \alpha_{t-1}^i)^2 \tag{4.12}$$

applied on the variation of the α_i. It serves to penalize policies that shift very abruptly between stabilization and movement commands.

4.3.2 H-RL vs. NH-RL

We compare the average accumulated reward achieved by NH-RL and by our proposed hierarchical decomposition H-RL, respectively represented by the blue and orange curves in Fig. 4.6. Results show that H-RL performs better or on par with NH-RL for all objects. For larger objects such as the football, the screwdriver box and the chips can, exploratory actions that cause the object to shift in-hand are not as detrimental to the learning episode, as the size of the object allows it to be re-grasped before being dropped. This behavior is shown by a clear correlation between the difference in performance of the two approaches and the size of the object and/or the number of fingers involved in the manipulation action. The impact of bad exploratory actions on the learning process increases as the objects size decreases, rendering NH-RL unable to learn movement policies for smaller objects, while H-RL can learn movement policies for all objects. Moreover, these results are additionally emphasized by the evolution of the trajectory length (number of actions taken before the object is dropped or the maximum number of actions is reached) during learning, shown in Fig. 4.7. The average trajectory length for NH-RL policies remains very close to zero in all experiments with smaller objects, where exploratory actions have a critical effect on the movement. In addition to size, the initial grasp configurations can also greatly influence the outcome of the learning. This is the case for the football and the baseball, where one of the fingers is slightly underneath the object as depicted in Fig. 4.8, serving as support for the exploration actions.

The effectiveness of the policies learned by both approaches also substantially differs. While NH-RL is capable of learning policies for the partially supported and for the larger objects, the resulting policies are only capable of maintaining the objects in-hand without any consistent movement towards the target pose. In contrast, the H-RL policies are capable of consistently reorienting the objects to the correct orientations, despite maintaining the initial position error. This behavior, shown in Fig. 4.9 for the lego block, is observed for both the cubic objects and the cylindrical objects. The spherical objects are on kept stable in-hand, with no consistent reduction of position or orientation errors. This behavior results from all the contacts being simulated as contacts between fully rigid objects. This form of contact simulation is particularly

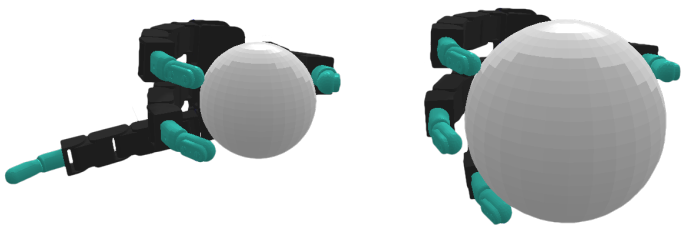

(a) (b)

Figure 4.8.: Initial grasps for (a) the baseball and (b) the mini football. In both cases, one of the fingers is slightly under one of the spheres, acting as a supporting surface and minimizing the effects of the exploratory actions.

relevant for spherical objects where very fine contact management is necessary for repositioning the object.
Finally, we show the effects of the F term enforcement, where we wish to keep all fingers of the initial grasps involved in the manipulation action. The evolution of the F term with the learning process shown in Fig. 4.10 indicates that the ratio between initial and used fingers increases with the number of episodes, converging to values near the maximum value of one, where all fingers in the initial grasp take part in the manipulation action.

4.3.3 Transfer on the real robot.

Several policies were tested on the real robot in order to assess their transfer capabilities. In Fig. 4.11, the movements produced by two policies for the lego block are depicted. Policies transferred with no further learning on the real robot, displaying similar movements to the ones observed in the simulation environment. While policies correctly transfer to the real robot, the movements are hindered by inaccuracies in the estimated contact normal and by noise on the slip predictors. These estimations are fairly robust for small movements but quickly diverge once contact positions considerably shift. This behavior results in policies executing the desired movements but, once the movement imposed by the upper level policy finishes, and most of the control response is attributed to the stabilizers, the object often is dropped from the grasp. This can potentially be improved by using more advanced normal estimation methods.

4.4 Conclusion

We have proposed a hierarchical decomposition for the in-hand manipulation problem in order to enable learning policies for manipulating unsupported objects. The

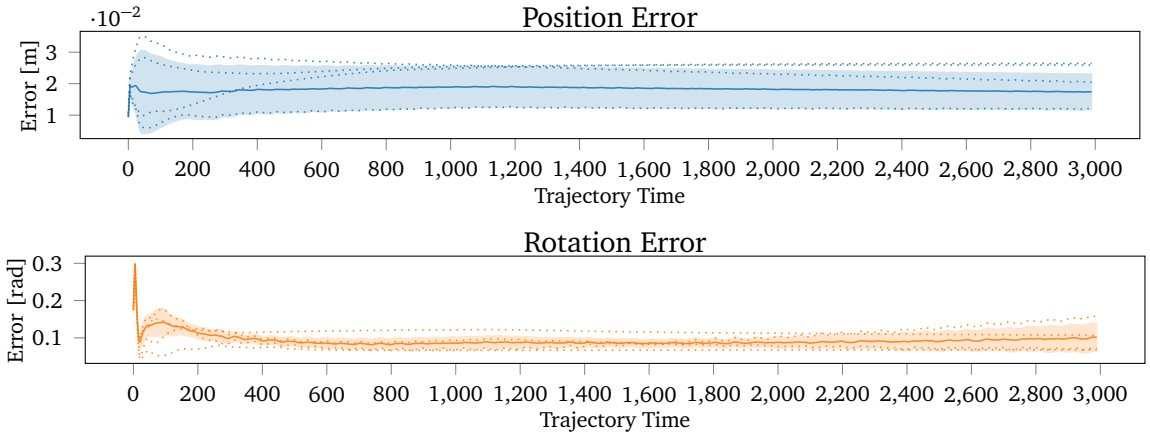

Figure 4.9.: The average behavior of the H-RL movement policies for the lego. The solid lines represent mean and the dashed lines the individual trials. While the position error is maintained throught the movement execution, the orientation error is consistently reduced.

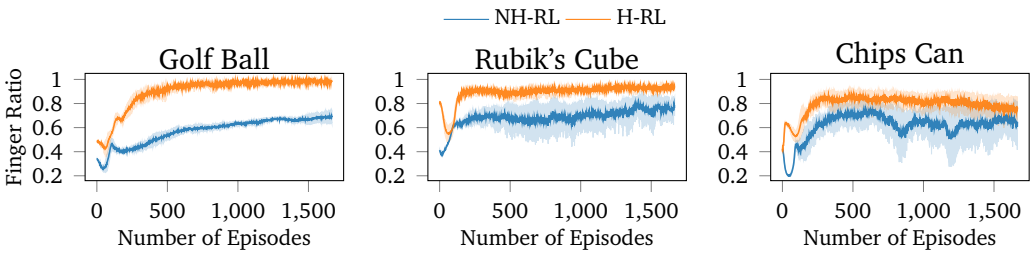

Figure 4.10.: Evolution of the F enforcement term with the learning episodes. With F converging to one, all fingers that compose the initial grasp are maintained throughout the duration of the movement trajectory.

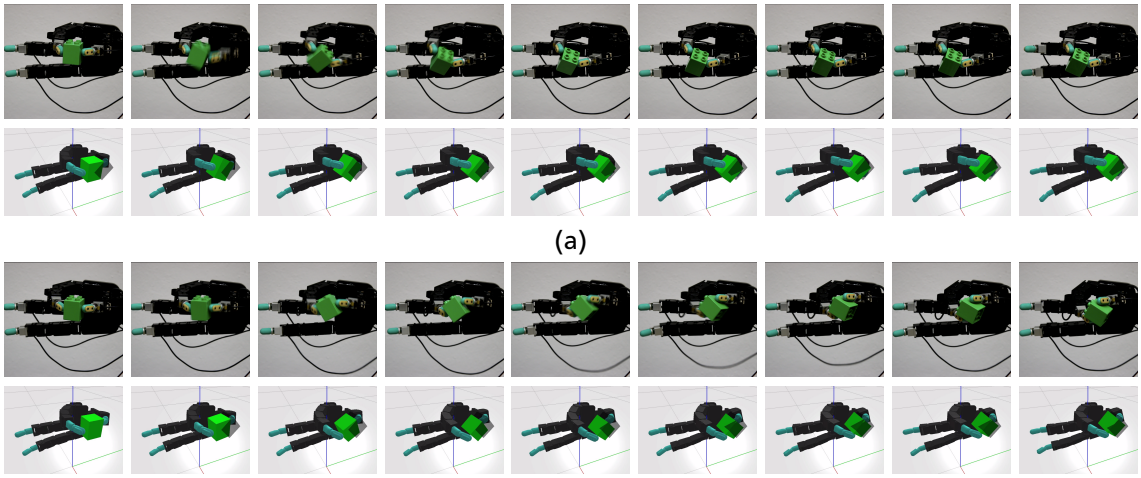

Figure 4.11.: The behavior of two policies trained on the simulator and transferred to the real robot with no additional training. The movements consist of a clockwise (a) or counter clockwise rotation of the object along the axis perpendicular to the palm.

policies learned in simulation were transferred to a real robot platform where similar manipulation movements are observed. Our decomposition is based on low-level per-digit stabilizing controllers that effectively incorporate tactile feedback to ensure a stable grip during object manipulation and a high-level policy that coordinates digit movement and modulates the influence of the individual low-level controllers. Our decomposition allows for efficient training of high-level policies for dexterous manipulation in simulation on a range of different objects, achieving faster learning and higher rewards than its non-hierarchical counterpart. By abstracting and encapsulating tactile feedback in the lower-level controllers, the hierarchical decomposition enables direct transfer of policies that were trained in simulation to a physical system. An interesting direction for future work is to explore the possibility of learning a single policy that is able to perform all achievable translations and rotations of the grasped object by taking inspiration from recent developments in multi-task reinforcement learning.

5 Conclusion

In this thesis we have presented several methods for improving the dexterous in-hand manipulation skills of robots. Here we provide a summarized version of each of these methods as well as potential future work directions.

5.1 Summary

As a first step towards dexterous in-hand manipulation, we begun by presenting an approach for predicting slip from high dimensional tactile information in Chapter 2. The predictors allow stabilization controllers to avoid the occurrence of slip via anticipatory reactions, improving the stability rates when compared to slip detection based stabilization controllers that react to slip after it occurs. We showcased the relevance of each tactile information channels for the prediction of slip and showed that the predicted slip signals can generalize across multiple objects, allowing the controllers to stabilize previously unknown objects. Finally, we showed that the predicted slip signals are robust to noise by having an object be jointly stabilized between a human and a robot.

Using the proposed slip predictors, and moving to a multi-finger setting, in Chapter 3 we showed that stable multi-fingered grasps can emerge from a set of independently controlled fingers. We demonstrated how, despite no explicit coordination between the finger controllers, coordinated stabilization movements emerged as each controller uses its tactile feedback to perceive perturbations that compromise the stability of its own interaction with the object. With each controller optimizing local stability and by ensuring smooth responses for each of the individual controllers, several objects were stabilized in-hand, with no required changes to the individual controllers when changing object and no enforcement of a specific grasp pose or of a specific force distribution between fingers. The reactive nature of the controllers makes the achieved grips very robust to external perturbations applied to the object or to the fingers and simple in-hand manipulations were demonstrated in a master-slave context, where a human master perturbs the fingers in order for the object to be manipulated while the individual grip stabilizers ensure the object is not dropped.

Following the results achieved via the master-slave operation in Chapter 3, we proposed a hierarchical control decomposition for the in-hand manipulation problem, which we have presented in Chapter 4. The hierarchy is composed of two controlled layers, high-level movement policy learned through reinforcement learning and a low-level composed of a set of independent grip stabilization controllers. We show that the proposed decomposition enables the learning of complex movements in scenarios where non-hierarchical reinforcement learning fails to learn. In addition, the low-level controllers function as an abstraction layer for the tactile information acquired by the sensors, and the design of similar low-level controllers in simulated

environments was shown to enable the transfer of high-level polices learned in simulation directly to the real platforms.
The combined methods proposed in this thesis demonstrate a successful integration of rich tactile information onto the feedback loop of dexterous in-hand manipulation control policies. While not a complete solution for the problem, the presented efforts focused on generalization, robustness and addressing the full complexity of the problem, aspects we believe to be crucial to achieve a general and complete solution to dexterous in-hand manipulation.

5.2 Future Work

While several possible avenues for future work can be considered, considering the previously presented methods, further exploration of tactile information can be considered the most general direction. While currently all approaches revolve around the prediction of slip, other types of information provided by the sense of touch are not considered. Information on other events such as making or breaking contact, as well as estimated object properties could be useful for all control hierarchy levels. The same hierarchy that benefits from the additional tactile information, allows the full complexity of the dexterous in-hand manipulation problem to be distributed, hence facilitating the integration of higher dimensional tactile signals in lower layers without overbearing consequences. Thus, hierarchical control schemes and the integration of increasingly rich tactile information seem to mutually benefit each other while jointly contributing for general dexterous in-hand manipulation tasks.
More specific research avenues are also considered. For completely reorienting an object in-hand, manipulation policies might have to consider breaking the contact between the objects and a subset of the involved fingers in order to reposition these fingers in such a way that the manipulation range is amplified. This commonly denoted as finger gaiting and is currently not explored in our learned movement policies. Despite this, the modular nature of the individual controllers that compose the low-level of our hierarchy as been shown to cope with such behaviors in the master-slave experiments.
Another interesting aspect to be explored is the interaction between the control levels in the hierarchy. This refers not only to which tactile data should be passed on from the lower-level layers to the upper levels but also considering using anticipatory and inhibitory signals between layers. As an example, during a manipulation movement, the movement policies might want to partially inhibit the grip stabilizers from increasing force, as the perturbations applied on the object are not to be considered undesired. On the other hand, anticipatory signals should be passed onto the the stabilizer as the desired manipulation is ending, to guarantee object stability post manipulation.
Finally, exploring other methodologies that allow all levels of the hierarchy to be adjusted, both on real and simulated environments, would allow for more synchronous control to emerge between all control layers while still ensuring that several of these layers can be modular in design.

A Publication List

A.1 Journal Papers

2018 Grip Stabilization of Novel Objects using Slip Prediction
Veiga, F. F.; Peters, J.; Hermans
IEEE Transactions on Haptics

A.2 Conference Papers

2018 Regularizing Reinforcement Learning with State Abstraction
Akrour, R.; **Veiga, F.F.**; Peters, J.; Neuman, G.
Proceedings of the IEEE/RSJ Conference on Intelligent Robots and Systems (IROS)

2018 Inducing Probabilistic Context-Free Grammars for the Sequencing of Robot Movement Primitives
Lioutikov, R.; Maeda, G.; **Veiga, F.F.**; Kersting, K.; Peters, J.
Proceedings of the International Conference on Robotics and Automation (ICRA)

2016 Active Tactile Object Exploration with Gaussian Processes
Yi, Z.; Calandra, R.; **Veiga, F. F.**; van Hoof, H.; Hermans, T.; Zhang, Y.; Peters
Proceedings of the IEEE/RSJ Conference on Intelligent Robots and Systems (IROS)

2015 Stabilizing Novel Objects by Learning to Predict Tactile Slip
Veiga, F.F.; van Hoof, H.; Peters, J.; Hermans, T.
Proceedings of the IEEE/RSJ Conference on Intelligent Robots and Systems (IROS)

A.3 Submitted

2018 Hierarchical Control Decomposition of Dexterous In-Hand Manipulation Tasks
Veiga, F. F.; Akrour, R.; Ranftl, R.; Dosovitskiy, A.; Koltun, V.; Peters, J.
Submitted to Frontiers in Robotics and AI

2018 In-Hand Object Stabilization by Independent Finger Control
Veiga, F. F.; Edin B.B; Peters, J.
Submitted to Advanced Robotics Journal

A.4 Pre-Prints

2016 Can Modular Finger Control for In-Hand Object Stabilization be accomplished by Independent Tactile Feedback Control Laws?
Veiga, F.F.; Peters, J.
arXiv

A.5 Workshop Papers

2014 Demonstration: Learning for Tactile Manipulation
Hermans, T.; **Veiga, F. F.**; Hölscher, J.; van Hoof, H.; Peters, J.
Advances in Neural Information Processing Systems (NIPS), Demonstration Track, MIT Press

2013 Active tactile exploration for grasping
Veiga, F. F.; Bernardino, A.
Proceedings of the ICRA 2013 Workshop on Autonomous Learning

2012 Towards Bayesian Grasp Optimization with Wrench Space Analysis
Veiga, F. F.; Bernardino, A.
Proceedings of the IROS 2012 Workshop Beyond Robot Grasping

B Curriculum Vitae

Education

2013 – present	Ph.D. student at the Intelligent Autonomous Systems Group Technical University Darmstadt, Darmstadt, Germany
2004 – 2012	Integrated M.Sc. in Electrical and Computer Engineering Instituto Superior Técnico, University of Lisbon, Portugal Thesis: Robotic Grasp Optimization from Contact force analysis Supervisors: Prof. A. Bernardino and Prof. J. Santos Victor

Summer Schools

2015	Human Sensing and Applications to Robotics and Haptic Displays Summer School Université Lille, Lille, France
2015	Machine Learning Summer School Kyoto University, Kyoto, Japan

Workshop Organization

2018	RoboTac: New Progress in Tactile Perception and Learning in Robotics Kaboli, M.; Bohg, J.; Li, Q.; **Veiga, F.F**, Su, Z.; Cheng, G. IEEE/RSJ International Conference on Intelligent Robots and Systems Madrid, Spain
2018	Multi-Modal Perception and Control **Veiga, F. F.**; Calandra, R.; Billard, A.; Peters, J. Robotics: Science and Systems Pittsburgh, USA
2016	Tactile Sensing for Manipulation: New Progress and Challenges Li, Q; Cherubini, A; Natale, L; Ho, V. A.; Su, Z.; **Veiga F. F.** IEE-RAS International Conference on Humanoid Robots Cancun, Mexico

Teaching Experience

Summer 2016	Teaching Assistant for Statistical Machine Learning
Winter 2015/2016	Teaching Assistant for Robot Learning

Student Supervision

Bachelor Thesis

2018 Guided Policy Search for In-Hand Manipulation
Schneider, T.; **Veiga, F.F**; Abdulsamad, H.; Peters, J.
Technical University Darmstadt

2017 Can we predict grasp forces from photos?
Heppert, N.; **Veiga, F.F.**; Goesele, M.; Peters, J.
Technical University Darmstadt

2014 Tactile Sensing for Manipulation
Huhnstock, N.; **Veiga, F.F.**; van Hoof, H.; Peters, J.
Technical University Darmstadt

Student Projects

2018 Deep Reinforcement Learning for playing Starcraft II
Palenicek, D.; Hussing, M.; Meister, S; **Veiga, F.F.**; Peters, J.
Technical University Darmstadt

2015 Contact Location Forward Modeling of BioTac Skin-like Data for Contact Location Control
Hesse, T.; Notz, D.; **Veiga, F.F.**; Peters, J.
Technical University Darmstadt

Reviewing

International Conferences

2018	Eurohaptics
2015-2018	IEEE International Conference on Robotics and Automation
2014-2018	IEEE-RAS International Conference on Humanoid Robots
2014-2017	IEEE/RSJ International Conference on Intelligent Robots and Systems

Journals

IEEE Transactions on Robotics

IEEE Robotics and Automation Letters

Robotics and Autonomous Systems

List of Figures

Bibliography

[1] Arash Ajoudani et al. *Reflex control of the Pisa/IIT softHand during object slippage*. In: *IEEE International Conference on Robotics and Automation (ICRA)*. IEEE. 2016, pp. 1972–1979.

[2] Yunfei Bai and C Karen Liu. *Dexterous manipulation using both palm and fingers*. In: *Robotics and Automation (ICRA), 2014 IEEE International Conference on*. IEEE. 2014, pp. 1560–1565.

[3] Yasemin Bekiroglu et al. *Assessing grasp stability based on learning and haptic data*. In: *IEEE Transactions on Robotics* 27.3 (2011), pp. 616–629.

[4] A. Bicchi and V. Kumar. *Robotic Grasping and Contact: A Review*. In: *IEEE International Conference on Robotics and Automation (ICRA)*. 2000, pp. 348–353.

[5] J. Bohg et al. *Data-Driven Grasp Synthesis: A Survey*. In: *IEEE Transactions on Robotics* 30.2 (2014), pp. 289–309.

[6] Jeannette Bohg et al. *Data-driven grasp synthesisa survey*. In: *IEEE Transactions on Robotics* 30.2 (2014), pp. 289–309.

[7] David L Brock. *Enhancing the dexterity of a robot hand using controlled slip*. In: *IEEE International Conference on Robotics and Automation (ICRA)*. 1988, pp. 249–251.

[8] Christopher JC Burges. *A tutorial on support vector machines for pattern recognition*. In: *Data mining and knowledge discovery* 2.2 (1998), pp. 121–167.

[9] Magnus KO Burstedt, J Randall Flanagan, and Roland S Johansson. *Control of grasp stability in humans under different frictional conditions during multidigit manipulation*. In: *Journal of neurophysiology* 82.5 (1999), pp. 2393–2405.

[10] MKO Burstedt, Benoni B Edin, and Roland S Johansson. *Coordination of fingertip forces during human manipulation can emerge from independent neural networks controlling each engaged digit*. In: *Experimental brain research* 117.1 (1997), pp. 67–79.

[11] Roberto Calandra et al. *The Feeling of Success: Does Touch Sensing Help Predict Grasp Outcomes?* In: *arXiv preprint arXiv:1710.05512* (2017).

[12] Berk Calli et al. *The YCB object and model set: Towards common benchmarks for manipulation research*. In: *Advanced Robotics (ICAR), 2015 International Conference on*. IEEE. 2015, pp. 510–517.

[13] Gaetano Canepa et al. *Detection of incipient object slippage by skin-like sensing and neural network processing*. In: *IEEE Transactions on Systems, Man, and Cybernetics, Part B (Cybernetics)* 28.3 (1998), pp. 348–356.

[14] Nikhil Chavan-Dafle and Alberto Rodriguez. *Prehensile pushing: In-hand manipulation with push-primitives*. In: *Intelligent Robots and Systems (IROS), 2015 IEEE/RSJ International Conference on*. IEEE. 2015, pp. 6215–6222.

[15] Moëz Cherif and Kamal K Gupta. *Planning quasi-static fingertip manipulations for reconfiguring objects*. In: *IEEE Transactions on Robotics and Automation* 15.5 (1999), pp. 837–848.

[16] Vivian Chu et al. *Using robotic exploratory procedures to learn the meaning of haptic adjectives*. In: *IEEE International Conference on Robotics and Automation (ICRA)*. 2013, pp. 3048–3055. ISBN: 978-1-4673-5643-5.

[17] Erwin Coumans and Yunfei Bai. *PyBullet, a Python module for physics simulation for games, robotics and machine learning*. `http://pybullet.org`. 2016–2018.

[18] A Criminisi, J Shotton, and E Konukoglu. *Decision forests for classification, regression, density estimation, manifold learning and semi-supervised learning*. In: *Microsoft Research Cambridge, Tech. Rep. MSRTR-2011-114* 5.6 (2011).

[19] Mark R Cutkosky, Robert D Howe, and William R Provancher. *Force and tactile sensors*. In: *Springer Handbook of Robotics* (2008), pp. 455–476.

[20] Nikhil Chavan Dafle et al. *Extrinsic dexterity: In-hand manipulation with external forces*. In: *Robotics and Automation (ICRA), 2014 IEEE International Conference on*. IEEE. 2014, pp. 1578–1585.

[21] Hao Dang and Peter K. Allen. *Stable grasping under pose uncertainty using tactile feedback*. In: *Autonomous Robots* 36.4 (2014), pp. 309–330.

[22] Hao Dang and Peter K Allen. *Stable grasping under pose uncertainty using tactile feedback*. In: *Autonomous Robots* 36.4 (2014), pp. 309–330.

[23] Prafulla Dhariwal et al. *OpenAI Baselines*. `https://github.com/openai/baselines`. 2017.

[24] Siyuan Dong, Wenzhen Yuan, and Edward Adelson. *Improved gelsight tactile sensor for measuring geometry and slip*. In: *arXiv preprint arXiv:1708.00922* (2017).

[25] Benoni B Edin, Göran Westling, and Roland S Johansson. *Independent control of human finger-tip forces at individual digits during precision lifting*. In: *The Journal of physiology* 450.1 (1992), pp. 547–564.

[26] Jeremy Fishel and Gary Lin. *BioTac® Product Manual*. In: ().

[27] Jeremy A Fishel. *Design and Use of a Biomimetic Tactile Microvibration Sensor with Human-Like Sensitivity and its Application in Texture Discrimination using Bayesian Exploration*. PhD thesis. University of Southern California, 2012.

[28] J Randall Flanagan, Magnus KO Burstedt, and Roland S Johansson. *Control of fingertip forces in multidigit manipulation*. In: *Journal of neurophysiology* 81.4 (1999), pp. 1706–1717.

[29] Isao Fujimoto et al. *Development of artificial finger skin to detect incipient slip for realization of static friction sensation*. In: *IEEE International Conference on Multisensor Fusion and Integration for Intelligent Systems (MFI)*. IEEE. 2003, pp. 15–20.

[30] Pedro Silva Girão et al. *Tactile sensors for robotic applications*. In: *Measurement* 46.3 (2013), pp. 1257–1271.

[31] Abhishek Gupta et al. *Learning dexterous manipulation for a soft robotic hand from human demonstrations*. In: *Intelligent Robots and Systems (IROS), 2016 IEEE/RSJ International Conference on*. IEEE. 2016, pp. 3786–3793.

[32] Charlotte Häger-Ross, Kelly J Cole, and Roland S Johansson. *Grip-force responses to unanticipated object loading: load direction reveals body-and gravity-referenced intrinsic task variables*. In: *Experimental Brain Research* 110.1 (1996), pp. 142–150.

[33] Katharina Hertkorn, Maximo A Roa, and Christoph Borst. *Planning in-hand object manipulation with multifingered hands considering task constraints*. In: *Robotics and Automation (ICRA), 2013 IEEE International Conference on*. IEEE. 2013, pp. 617–624.

[34] Barrett Heyneman and MR Cutkosky. *Slip interface classification through tactile signal coherence*. In: *IEEE/RSJ International Conference on Intelligent Robotics and Systems (IROS)*. 2013, pp. 801–808.

[35] Van Anh Ho et al. *What can be inferred from a tactile arrayed sensor in autonomous in-hand manipulation?* In: *2012 IEEE International Conference on Automation Science and Engineering (CASE)* (Aug. 2012), pp. 461–468. DOI: 10.1109/CoASE.2012.6386384.

[36] Koh Hosoda, Yasunori Tada, and Minoru Asada. *Anthropomorphic robotic soft fingertip with randomly distributed receptors*. In: *Robotics and Autonomous Systems* 54.2 (2006), pp. 104–109.

[37] Robert D Howe and Mark R Cutkosky. *Sensing skin acceleration for slip and texture perception*. In: *IEEE International Conference on Robotics and Automation (ICRA)*. IEEE. 1989, pp. 145–150.

[38] Atsutoshi Ikeda et al. *Grip force control for an elastic finger using vision-based incipient slip feedback*. In: *IEEE/RSJ International Conference on Intelligent Robotics and Systems (IROS)*. Vol. 1. 2004, pp. 810–815.

[39] Nawid Jamali and Claude Sammut. *Slip prediction using Hidden Markov models: Multidimensional sensor data to symbolic temporal pattern learning*. In: *IEEE International Conference on Robotics and Automation (ICRA)*. 2012, pp. 215–222.

[40] Roland Johansson. *The Effects of Anesthesia on Motor Skills - Youtube*. URL: https://www.youtube.com/watch?v=0LfJ3M3Kn80.

[41] Roland S Johansson and J Randall Flanagan. *Coding and use of tactile signals from the fingertips in object manipulation tasks.* In: *Nature Reviews Neuroscience* 10.5 (May 2009), pp. 345–59. ISSN: 1471-0048. DOI: 10.1038/nrn2621.

[42] Roland S Johansson and AB Vallbo. *Tactile sensibility in the human hand: relative and absolute densities of four types of mechanoreceptive units in glabrous skin.* In: *The Journal of physiology* 286.1 (1979), pp. 283–300.

[43] Roland S Johansson and Goran Westling. *Roles of glabrous skin receptors and sensorimotor memory in automatic control of precision grip when lifting rougher or more slippery objects*. In: *Experimental brain research* 56.3 (1984), pp. 550–564.

[44] Roland S Johansson and Göran Westling. *Signals in tactile afferents from the fingers eliciting adaptive motor responses during precision grip*. In: *Experimental Brain Research* 66 (1987), pp. 141–154.

[45] Zhanat Kappassov, Juan-Antonio Corrales, and Véronique Perdereau. *Tactile sensing in dexterous robot hands*. In: *Robotics and Autonomous Systems* 74 (2015), pp. 195–220.

[46] Moslem Kazemi et al. *Robust Object Grasping Using Force Compliant Motion Primitives*. In: *Robotics: Science and Systems VIII* (2013), p. 177.

[47] William H Kruskal and W Allen Wallis. *Use of ranks in one-criterion variance analysis*. In: *Journal of the American statistical Association* 47.260 (1952), pp. 583–621.

[48] Vikash Kumar, Emanuel Todorov, and Sergey Levine. *Optimal control with learned local models: Application to dexterous manipulation*. In: *Robotics and Automation (ICRA), 2016 IEEE International Conference on*. IEEE. 2016, pp. 378–383.

[49] Susan J Lederman and Roberta L Klatzky. *Haptic perception: A tutorial*. In: *Attention, Perception, & Psychophysics* 71.7 (2009), pp. 1439–1459.

[50] Nathan F Lepora and Benjamin Ward-Cherrier. *Superresolution with an optical tactile sensor*. In: *2015 IEEE/RSJ International Conference on Intelligent Robots and Systems (IROS)*. IEEE. 2015, pp. 2686–2691.

[51] Sergey Levine et al. *End-to-End Training of Deep Visuomotor Policies*. In: *Journal of Machine Learning Research* 17 (2016).

[52] Miao Li et al. *Learning of Grasp Adaptation through Experience and Tactile Sensing*. In: *IEEE/RSJ International Conference on Intelligent Robotics and Systems (IROS)*. 2014, pp. 3339–3346.

[53] Miao Li et al. *Learning of grasp adaptation through experience and tactile sensing*. In: *IEEE/RSJ International Conference on Intelligent Robotics and Systems (IROS)*. Ieee. 2014, pp. 3339–3346.

[54] Raymond R Ma and Aaron M Dollar. *On dexterity and dexterous manipulation*. In: *Advanced Robotics (ICAR), 2011 15th International Conference on*. IEEE. 2011, pp. 1–7.

[55] Marianna Madry et al. *ST-HMP: Unsupervised spatio-temporal feature learning for tactile data*. In: *IEEE International Conference on Robotics and Automation (ICRA)*. 2014, pp. 2262–2269.

[56] Marianna Madry et al. *ST-HMP: Unsupervised spatio-temporal feature learning for tactile data*. In: *IEEE International Conference on Robotics and Automation (ICRA)*. IEEE. 2014, pp. 2262–2269.

[57] Hitoshi Maekawa, Kazuo Tanie, and Kiyoshi Komoriya. *Tactile sensor based manipulation of an unknown object by a multifingered hand with rolling contact*. In: *Robotics and Automation, 1995. Proceedings., 1995 IEEE International Conference on*. Vol. 1. IEEE. 1995, pp. 743–750.

[58] Alexis Maldonado, Humberto Alvarez, and Michael Beetz. *Improving robot manipulation through fingertip perception*. In: *IEEE/RSJ International Conference on Intelligent Robotics and Systems (IROS)*. Oct. 2012, pp. 2947–2954. ISBN: 978-1-4673-1736-8. DOI: 10.1109/IROS.2012.6385560.

[59] Claudio Melchiorri. *Slip detection and control using tactile and force sensors*. In: *IEEE/ASME Transactions on Mechatronics* 5.3 (2000), pp. 235–243.

[60] Volodymyr Mnih et al. *Human-level control through deep reinforcement learning*. In: *Nature* 518.7540 (Feb. 2015), pp. 529–533.

[61] Igor Mordatch, Zoran Popović, and Emanuel Todorov. *Contact-invariant optimization for hand manipulation*. In: *Proceedings of the ACM SIGGRAPH/Eurographics symposium on computer animation*. Eurographics Association. 2012, pp. 137–144.

[62] Allison M Okamura, Niels Smaby, and Mark R Cutkosky. *An overview of dexterous manipulation*. In: *Robotics and Automation, 2000. Proceedings. ICRA'00. IEEE International Conference on*. Vol. 1. IEEE. 2000, pp. 255–262.

[63] OpenAI et al. *Learning Dexterous In-Hand Manipulation*. In: (2018). arXiv: 1808.00177.

[64] Xiao-Dong Pang, Hong Z Tan, and Nathaniel I Durlach. *Manual discrimination of force using active finger motion*. In: *Perception & psychophysics* 49.6 (1991), pp. 531–540.

[65] Alexandros Paraschos et al. *Probabilistic movement primitives*. In: *Advances in neural information processing systems*. 2013, pp. 2616–2624.

[66] Fabian Pedregosa and G Varoquaux. *Scikit-learn: Machine learning in Python*. In: *Journal of Machine Learning Research* 12 (2011), pp. 2825–2830.

[67] Lerrel Pinto and Abhinav Gupta. *Supersizing self-supervision: Learning to grasp from 50k tries and 700 robot hours*. In: *Robotics and Automation (ICRA), 2016 IEEE International Conference on*. IEEE. 2016, pp. 3406–3413.

[68] Ivaylo Popov et al. *Data-efficient deep reinforcement learning for dexterous manipulation*. In: *arXiv preprint arXiv:1704.03073* (2017).

[69] Domenico Prattichizzo et al. *On motion and force controllability of precision grasps with hands actuated by soft synergies*. In: *IEEE transactions on robotics* 29.6 (2013), pp. 1440–1456.

[70] S. Lederman R. Klatzky R. Bajcsy. *Object exploration in one and two fingered robots*. In: *IEEE International Conference on Robotics and Automation (ICRA)*. 1987.

[71] Aravind Rajeswaran et al. *Learning complex dexterous manipulation with deep reinforcement learning and demonstrations*. In: *arXiv preprint arXiv:1709.10087* (2017).

[72] Jens Reinecke, Alexander Dietrich, and Florian Schmidt. *Experimental Comparison of Slip Detection Strategies by Tactile Sensing with the BioTac on the DLR Hand Arm System*. In: *IEEE International Conference on Robotics and Automation (ICRA)* (2014), pp. 2742–2748.

[73] Joseph M Romano et al. *Human-Inspired Robotic Grasp Control With Tactile Sensing*. In: *IEEE Transactions on Robotics* 27.6 (2011), pp. 1067–1079.

[74] Joseph M Romano et al. *Human-inspired robotic grasp control with tactile sensing*. In: *IEEE Transactions on Robotics* 27.6 (2011), pp. 1067–1079.

[75] Jean-Philippe Saut et al. *Dexterous manipulation planning using probabilistic roadmaps in continuous grasp subspaces*. In: *Intelligent Robots and Systems, 2007. IROS 2007. IEEE/RSJ International Conference on*. IEEE. 2007, pp. 2907–2912.

[76] John Schulman et al. *Trust Region Policy Optimization*. In: *International Conference on Machine Learning (ICML)* (2015), p. 16.

[77] Matthias Shöpfer et al. *Using a Piezo-Resistive Tactile Sensor for Detection of Incipient Slippage*. In: *International Symposium on Robotics (ISR) and German Conference on Robotics (ROBOTIK)*. 2010.

[78] David Silver et al. *Mastering the Game of Go with Deep Neural Networks and Tree Search*. In: *Nature* 529.7587 (Jan. 2016), pp. 484–489.

[79] Xiaojing Song et al. *A novel dynamic slip prediction and compensation approach based on haptic surface exploration*. In: *IEEE/RSJ International Conference on Intelligent Robotics and Systems (IROS)*. IEEE. 2012, pp. 4511–4516.

[80] Johannes A Stork et al. *Learning predictive state representation for in-hand manipulation*. In: *Robotics and Automation (ICRA), 2015 IEEE International Conference on*. IEEE. 2015, pp. 3207–3214.

[81] Zhe Su et al. *Force Estimation and Slip Detection for Grip Control using a Biomimetic Tactile Sensor*. In: *IEEE/RAS International Conference on Humanoid Robots (Humanoids)*. 2015, pp. 297–303.

[82] Balakumar Sundaralingam and Tucker Hermans. *Relaxed-rigidity constraints: kinematic trajectory optimization and collision avoidance for in-grasp manipulation*. In: *Autonomous Robots* (2018), pp. 1–15.

[83] Yasunori Tada and Koh Hosoda. *Acquisition of multi-modal expression of slip through pick-up experiences*. In: *Advanced Robotics* 21.5-6 (2007), pp. 601–617.

[84] M.R. Tremblay and M.R. Cutkosky. *Estimating friction using incipient slip sensing during a manipulation task*. In: *IEEE International Conference on Robotics and Automation (ICRA)*. 1993, 429–434 vol.1.

[85] Herke Van Hoof et al. *Learning robot in-hand manipulation with tactile features*. In: *Humanoid Robots (Humanoids), 2015 IEEE-RAS 15th International Conference on*. IEEE. 2015, pp. 121–127.

[86] Filipe Veiga, Benoni B. Edin, and Jan Peters. *In-Hand Object Stabilization by Independent Finger Control*. In: *arXiv preprint arXiv:1806.05031* (2018).

[87] Filipe Veiga et al. *Stabilizing Novel Objects by Learning to Predict Tactile Slip*. In: *IEEE/RSJ International Conference on Intelligent Robotics and Systems (IROS)*. 2015, pp. 5065–5072.

[88] F Viña et al. *Predicting Slippage and Learning Manipulation Affordances through Gaussian Process Regression*. In: *IEEE/RAS International Conference on Humanoid Robots (Humanoids)*. 2013, pp. 462–468.

[89] G Westling and Roland S Johansson. *Responses in glabrous skin mechanoreceptors during precision grip in humans*. In: *Experimental brain research* 66.1 (1987), pp. 128–140.

[90] Nicholas Wettels, Jeremy A Fishel, and Gerald E Loeb. *Multimodal tactile sensor*. In: *The Human Hand as an Inspiration for Robot Hand Development*. Springer, 2014, pp. 405–429.

[91] Nicholas Wettels, Jeremy A Fishel, and Gerald E Loeb. *Multimodal tactile sensor*. In: *The Human Hand as an Inspiration for Robot Hand Development*. Springer, 2014, pp. 405–429.

[92] Nicholas Wettels et al. *Grip control using biomimetic tactile sensing systems*. In: *IEEE/ASME Transactions on Mechatronics* 14.6 (2009), pp. 718–723.

[93] X Alice Wu et al. *Incipient Slip Detection and Recovery for Controllable Gecko-Inspired Adhesion*. In: *IEEE Robotics and Automation Letters* 2.2 (2017), pp. 460–467.

[94] Ali Yahya et al. *Collective robot reinforcement learning with distributed asynchronous guided policy search*. In: *Intelligent Robots and Systems (IROS), 2017 IEEE/RSJ International Conference on*. IEEE. 2017, pp. 79–86.

[95] Akihiko Yamaguchi and Christopher G Atkeson. *Combining finger vision and optical tactile sensing: Reducing and handling errors while cutting vegetables*. In: *2016 IEEE-RAS 16th International Conference on Humanoid Robots (Humanoids)*. IEEE. 2016, pp. 1045–1051.

[96] Hanna Yousef, Mehdi Boukallel, and Kaspar Althoefer. *Tactile sensing for dexterous in-hand manipulation in roboticsâĂŤA review*. In: *Sensors and Actuators A: Physical* 167.2 (2011), pp. 171–187.

[97] Wenzhen Yuan, Siyuan Dong, and Edward Adelson. *Gelsight: High-resolution robot tactile sensors for estimating geometry and force*. In: *Sensors* 17.12 (2017), p. 2762.

[98] Xin-Zhi Zheng, Ryo Nakashima, and Tsuneo Yoshikawa. *On dynamic control of finger sliding and object motion in manipulation with multifingered hands*. In: *IEEE Transactions on Robotics and Automation* 16.5 (2000), pp. 469–481.